PERGAMON

International Journal of Solids and Structures 38 (2001) 1369–1394

INTERNATIONAL JOURNAL OF SOLIDS and STRUCTURES

www.elsevier.com/locate/ijsolstr

Electro-elastic stress analysis on piezoelectric inhomogeneity–crack interaction

Z.M. Xiao [a,*], J. Bai [a], R. Maeda [b]

[a] *School of Mechanical and Production Engineering, Nanyang Technological University, Nanyang Avenue, Singapore 639798, Singapore*
[b] *Mechanical Engineering Laboratory, Tsukuba, Ibaraki, Japan*

Received 13 June 1999; in revised form 6 March 2000

Abstract

The current study investigates the interaction problem of a fiber-shaped piezoelectric inhomogeneity embedded in a non-piezoelectric elastic matrix, which contains a crack. The matrix is assumed to be infinite in all directions and the crack is near the piezoelectric fiber. Different geometrical crack–inhomogeneity configurations are considered. The body is subjected to a far-field in-plane tension and a far-field anti-plane electric field. With the solution of stress field for a piezoelectric inhomogeneity embedded in an elastic matrix, the solution of current problem is obtained through a decomposition process. A set of singular integral equations in the crack domain is derived through the dislocation theory. The expressions for the stress intensity factors are then obtained in terms of the asymptotic values of dislocation density functions solved from these integral equations. Numerical examples indicate that interaction between the piezoelectric inhomogeneity and the crack is influenced by many factors, such as the configuration, the material properties of the piezoelectric inhomogeneity and matrix, as well as the far-field electrical and mechanical loadings. The stress intensity factors on crack tips obtained have been checked and confirmed by finite element analysis.

Keywords: Piezoelectric inhomogeneity; Crack; Interaction; Stress intensity factors

1. Introduction

Along with the widespread applications of piezoelectric materials and piezoelectric composites, the electro-elastic analysis of such materials becomes one of the most important problems in engineering. Due to their intrinsic electro-mechanical coupling behavior, piezoelectric materials have been widely used as resonators, actuators and sensors, among which sensor is the most common application. When piezoelectric materials are used as sensors, they are usually embedded in non-piezoelectric materials. Because of the electro-mechanical interaction between the sensor and the surrounding material, the properties of the surrounding material may influence the response of the sensor to external load. According to this phenomenon, the sensor can be used to detect possible defects in the surrounding material. So, it is desirable to

* Corresponding author. Tel.: +65-799-4726; fax: +65-791-1859.
E-mail address: mzxiao@ntu.edu.sg (Z.M. Xiao).

0020-7683/01/$ - see front matter
PII: S0020-7683(00)00096-2

understand the interaction between the piezoelectric sensor and a near-by flaw in the matrix. This is the main objective of the current investigation.

It is worthwhile to summarize the previous work directly related to present study in open literature. Extension of the well-known Eshelby (1957) ellipsoidal inhomogeneity solution for elasticity to piezoelectric material has been done by Wang (1992). Due to the complexity of the problem, conclusions drawn based on his formulation are general. In the three-dimensional formulation of Wang (1992), both the inhomogeneity and matrix are piezoelectric materials, and he reached the result that all the field variables are uniform inside the inclusion. However, the general anisotropy and coupling of mechanical and electrical fields have limited further extension of his work. Some simplification has to be made for a specific problem in order to gain an insight into the problem. When a piezoelectric material is used as a sensor, the matrix is most likely to be a non-piezoelectric material. Fan (1995) analyzed a piezoelectric ellipsoidal sensor embedded in a non-piezoelectric elastic matrix via equivalent inclusion method. The assumption of no electromechanical interaction in the matrix material simplified the formulation compared to Wang's work (1992). The original piezoelectric inhomogeneity problem is partially decoupled into an elastic problem and a dielectric problem connected via some "eigenstrain" and "eigenelectric field".

In our previous work, following Wang (1992) and Fan (1995), the stress field outside a piezoelectric inhomogeneity embedded in non-piezoelectric matrix is evaluated (Xiao and Bai, 1999a); then, the stress field and stress intensity factor for a Griffith crack located near a piezoelectric inhomogeneity are obtained for a simple crack–inhomogeneity configuration (Xiao and Bai, 1999b). The present study aims to extend the work of Xiao and Bai (1999b) to generalized inhomogeneity–crack geometric configuration, and give a generic solution method to piezoelectric inhomogeneity–crack interaction problem. It is worth mentioning that in the problem solved by Xiao and Bai (1999b), the crack is located symmetrically relative to the piezoelectric fiber sensor, no Mode II stress intensity factor exists at the crack tip. While for the current study, the analytical method developed can be applied to any general case that crack is located with random orientation near the piezoelectric sensor. As a result, the formulation here is much more complex and both Mode I and Mode II stress intensity factors exist at the crack tip. As mentioned in the beginning of this section, the engineering application of the current study is to use piezoelectric sensors to detect the possible near-by-micro crack. As the crack orientation is unknown in advance, the investigation in this paper can better serve the practical engineering application purpose.

2. Physical problem and decomposition process

The physical problem to be investigated is shown in Fig. 1(a), where the solid is assumed in a plane strain state. The matrix is an isotropic elastic material. The inhomogeneity is transversely isotropic piezoelectric material (with x_3 as the poling axis) in cylindrical shape with radius a and infinite length. The crack with length $2c$ is arbitrarily oriented on x_1x_2 plane. A parameter δ is used to denote the distance between the centers of the inhomogeneity and the crack. The matrix is subjected to a far-field in-plane uniform tension σ_{22}^0 and anti-plane electric field E_3^0. The coordinate used here is plane coordinate system (x_1, x_2) with the origin at the center of the inhomogeneity.

As the matrix is a purely elastic material, there is no mechanical-electric coupling behavior inside the matrix. By employing a superposition process (Hills et al., 1996), the original problem shown in Fig. 1(a) can be obtained through the sum of two sub-problems, as shown in Fig. 1(b) and (c), respectively. The problem shown in Fig. 1(b) is a piezoelectric inhomogeneity embedded in the matrix without the crack. The solution of this problem can be found in Xiao and Bai (1999a). For the second sub-problem shown in Fig. 1(c), the only external loads are the crack surface tractions which are equal in magnitude and opposite in sign to the stresses obtained in the problem Fig. 1(b) along the line which is the presumed location of the crack. The superposition of Fig. 1(b) and (c) is thus equal to the original problem in Fig. 1(a).

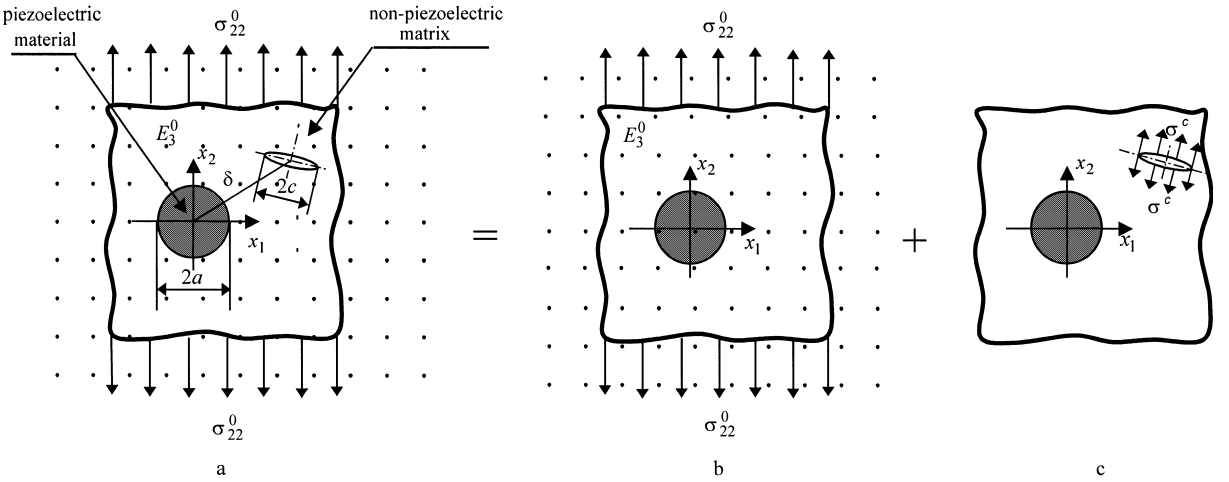

Fig. 1. The physical problem and the superposition procedure.

3. Stress intensity factor of the crack

The stress field due to the crack as shown in Fig. 1(c) can be simulated by a set of continuously distributed dislocations, and the stress intensity factors on the crack tips are evaluated through the dislocation density functions.

3.1. Integral equations

Based on Bueckner's theorem (Hills et al., 1996), the strategy of distributed dislocation technique is to produce a stress distribution equal to the tractions appearing along the crack faces by distributing dislocations along the crack line. The integral equation for the dislocation disturbance problem is obtained by using the solution of an edge dislocation interacting with a circular inhomogeneity.

As shown in Fig. 2(a), two edge dislocations with Burger's vector b_x and b_y are located at point A $(x = \xi, y = 0)$ on the crack line. The stresses induced at the point $P(x, y)$ in the matrix are found from the corresponding Airy stress functions (Dundurs and Mura, 1964), given by

$$\frac{\pi(k_0+1)}{G_0}\bar{\sigma}_{yy}(x,y,\xi) = h_{yy1}(x,y,\xi)b_x + h_{yy2}(x,y,\xi)b_y, \tag{1a}$$

$$\frac{\pi(k_0+1)}{G_0}\bar{\sigma}_{xx}(x,y,\xi) = h_{xx1}(x,y,\xi)b_x + h_{xx2}(x,y,\xi)b_y, \tag{1b}$$

$$\frac{\pi(k_0+1)}{G_0}\bar{\sigma}_{xy}(x,y,\xi) = h_{xy1}(x,y,\xi)b_x + h_{xy2}(x,y,\xi)b_y, \tag{1c}$$

where

$$h_{yy1} = -2\left(1-\frac{2x_1^2}{r_1^2}\right)\frac{y}{r_1^2} + \left(3A - B - 4A\frac{x_2^2}{r_2^2}\right)\frac{y}{r_2^2} - \left(3A - B - 4A\frac{x^2}{r^2}\right)\frac{y}{r^2} - 2A\frac{\beta^2-1}{\beta^3}\frac{a}{r_2^2}\left[-\frac{6x_2y}{r_2^2} + \frac{8x_2^3y}{r_2^4} + \frac{\beta^2-1}{\beta}\left(1-\frac{4x_2^2}{r_2^2}\right)\frac{ay}{r_2^2}\right] + \frac{B-A}{\beta}\frac{2xya}{r^4} + 2A\left(1-\frac{4x^2}{r^2}\right)\frac{a^2y}{r^4}, \tag{2a}$$

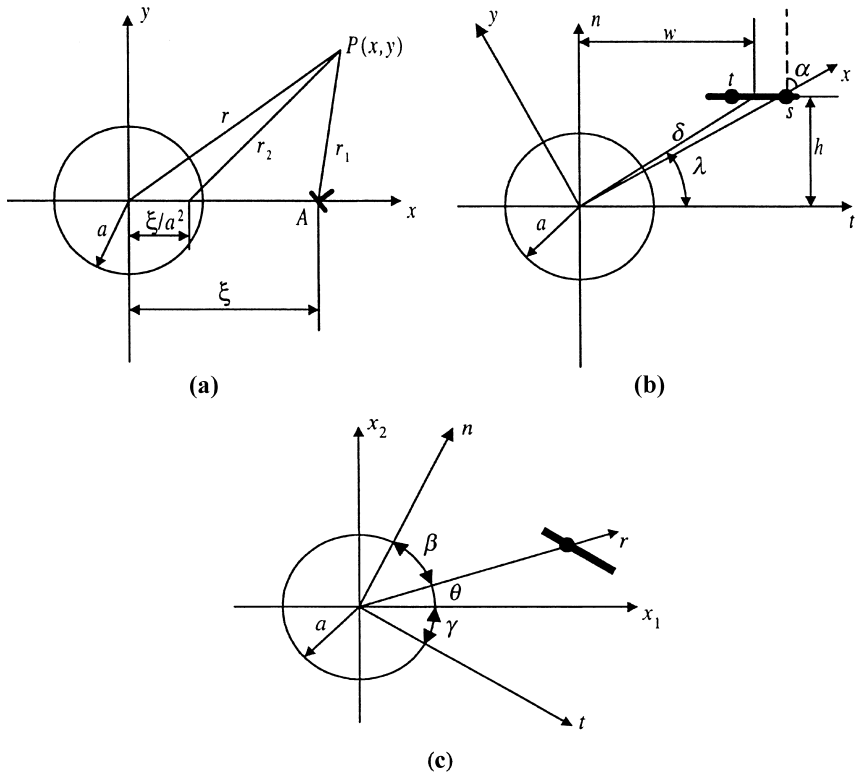

Fig. 2. The dislocations b_x and b_y, and the crack L in the neighborhood of a circular inhomogeneity.

$$h_{xx1} = -2\left(1+\frac{2x_1^2}{r_1^2}\right)\frac{y}{r_1^2} + \left[B + A\left(1+\frac{4x_2^2}{r_2^2}\right)\right]\frac{y}{r_2^2} - \left[B + A\left(1+\frac{4x^2}{r^2}\right)\right]\frac{y}{r^2} - 2\frac{B-A}{\beta}\frac{xya}{r^4} - 2A\left(1-\frac{4x^2}{r^2}\right)\frac{a^2y}{r^4} - A\frac{\beta^2-1}{\beta^3}\left[\left(1-\frac{4x_2^2}{r_2^2}\right)\frac{2x_2}{r} - \frac{\beta^2-1}{\beta}\left(1-\frac{4x_2^2}{r_2^2}\right)\frac{a}{r_2^2}\right]\frac{2ya}{r_2^2}, \tag{2b}$$

$$h_{xy1} = -2\left(1-\frac{2x_1^2}{r_1^2}\right)\frac{x_1}{r_1^2} + \left(3A - B - 4A\frac{x_2^2}{r_2^2}\right)\frac{x_2}{r_2^2} - \left(3A - B - 4A\frac{x^2}{r^2}\right)\frac{y}{r^2} - 2A\frac{\beta^2-1}{\beta^3}\frac{a}{r_2^2} \times \left[1 - \frac{8x_2^2}{r_2^2} + \frac{8x_2^4}{r_2^4} + \frac{\beta^2-1}{\beta}\left(3-\frac{4x_2^2}{r_2^2}\right)\frac{ax_2}{r_2^2}\right]\frac{a}{r_2^2} - \left(3A - B - 4A\frac{x_2}{r_2}\right)\frac{x}{r^2} - \frac{B-A}{\beta}\left(1-2\frac{x^2}{r^2}\right)\frac{a}{r_2^2} + 2A\left(3-\frac{4x^2}{r^2}\right)\frac{a^2x}{r^4}, \tag{2c}$$

$$h_{yy2} = 2\left(3-\frac{2x_1^2}{r_1^2}\right)\frac{x_1}{r_1^2} - \left(5A + B - 4A\frac{x_2^2}{r_2^2}\right)\frac{x_2}{r_2^2} + \left(5A + B - 4A\frac{x_2}{r_2}\right)\frac{x}{r^2} - A\frac{\beta^2-1}{\beta^3}\left[2(2-\beta^2) - 4(5-\beta^2)\frac{x_2^2}{r_2^2} + 16\frac{x_2^4}{r_2^4} + \frac{2(\beta^2-1)}{\beta}\left(3-4\frac{x_2^2}{r_2^2}\right)\frac{ax_2}{r_2^2}\right]\frac{a}{r_2^2} - 2A\left(3-\frac{4x^2}{r^2}\right)\frac{a^2x}{r^4} - \frac{1}{\beta}\left(1-\frac{2x^2}{r^2}\right)\frac{a}{r^2}\left[A(2\beta^2-1) + M(1+k_1) - 1\right], \tag{2d}$$

$$h_{xx2} = -2\left(1-\frac{2x_1^2}{r_1^2}\right)\frac{x_1}{r_1^2} + \left[B + A\left(1-\frac{4x_2^2}{r_2^2}\right)\right]\frac{x_2}{r_2^2} - \left[B + A\left(1-\frac{4x^2}{r^2}\right)\right]\frac{x}{r^2}$$
$$- A\frac{\beta^2-1}{\beta^3}\left[2\beta^2\left(1-\frac{2x_2^2}{r_2^2}\right) + 4\left(3-4\frac{x_2^2}{r_2^2}\right)\frac{x_2^2}{r_2^2} - \frac{2(\beta^2-1)}{\beta}\left(3-4\frac{x_2^2}{r_2^2}\right)\frac{ax_2}{r_2^2}\right]\frac{a}{r_2^2}$$
$$+ \left[A(2\beta^2-1) + M(1+k_1) - 1\right]\frac{1}{\beta}\left(1-\frac{2x^2}{r^2}\right)\frac{a}{r^2} + 2A\left(3-\frac{4x^2}{r^2}\right)\frac{a^2x}{r^4}, \tag{2e}$$

$$h_{xy2} = -2\left(1-\frac{2x_1^2}{r_1^2}\right)\frac{y}{r_1^2} + \left[B + A\left(1-\frac{4x_2^2}{r_2^2}\right)\right]\frac{y}{r_2^2} - \left[B + A\left(1-\frac{4x^2}{r^2}\right)\right]\frac{y}{r^2}$$
$$+ 2A\frac{\beta^2-1}{\beta^3}\left[\left(2\beta^2-4+8\frac{x_2^2}{r_2^2}\right)\frac{x_2y}{r_2^2} + \frac{\beta^2-1}{\beta}\left(1-\frac{4x_2^2}{r_2^2}\right)\frac{ay}{r_2^2}\right]\frac{a}{r_2^2}$$
$$- \left[A(2\beta^2-1)M(1+k_1) - 1\right]\frac{1}{\beta}\frac{2xya}{r^4} + 2A\left(1-\frac{4x^2}{r^2}\right)\frac{a^2y}{r^4}, \tag{2f}$$

$$k_0 = 3-4\nu_0, \qquad k_1 = 3-4\nu_1, \tag{3}$$

$$\beta = \frac{\xi}{a}, \qquad m = \frac{G_1}{G_0}, \qquad A = \frac{1-m}{1+mk_0}, \qquad B = \frac{k_1-mk_0}{k_1+m}, \qquad M = \frac{m(1+k_0)}{(m+k_1)(k_1-1+2m)}, \tag{4}$$

$$x_1 = x-\xi, \qquad x_2 = x-\frac{a^2}{\xi}, \qquad r^2 = x^2+y^2, \qquad r_1^2 = (x-\xi)^2+y^2, \qquad r_2^2 = \left(x-\frac{a^2}{\xi}\right)^2 + y^2. \tag{5}$$

Now, we assume that the tractions along the crack line L are generated by a set of continuously distributed dislocations. For convenience, a (t,n) Cartesian coordinate system is created here. It takes the center of the inhomogeneity as its origin with the t-axis parallel to the crack line L and the n-axis perpendicular to the crack line, as shown in Fig. 2(b). The distances from the center of the crack line to the n-axis and t-axis are w and h, respectively, i.e. $\delta = \sqrt{w^2+h^2}$. λ is the angle between t axis and the connection line between centers of the inhomogeneity and the crack. As defined in Fig. 1, the length of L is $2c$.

If $\alpha = \alpha(s)$ is the angle between the x-axis and the n-axis, noting that Eqs. (1a)–(1c) are also valid for $(x,y) \in L$ and the point $(\xi,0)$ corresponds to $t = s$ on L, the normal and tangential stresses on L due to dislocations b_x and b_y on L are as follows:

$$\sigma_{\mathrm{n}}^b = \bar{\sigma}_{xx}\cos^2\alpha + \bar{\sigma}_{yy}\sin^2\alpha + 2\bar{\sigma}_{xy}\sin\alpha\cos\alpha, \tag{6a}$$

$$\sigma_{\mathrm{t}}^b = (\bar{\sigma}_{yy} - \bar{\sigma}_{xx})\sin\alpha\cos\alpha + \bar{\sigma}_{xy}(\cos^2\alpha - \sin^2\alpha), \tag{6b}$$

where

$$\sin\alpha = \frac{s}{\sqrt{s^2+h^2}}, \qquad \cos\alpha = \frac{h}{\sqrt{s^2+h^2}}, \qquad x = \frac{h^2+ts}{\sqrt{s^2+h^2}}, \qquad y = \frac{h(s-t)}{\sqrt{s^2+h^2}},$$
$$x_1 = \frac{s(t-s)}{\sqrt{s^2+h^2}}, \qquad x_2 = \frac{ts+h^2-a^2}{\sqrt{s^2+h^2}}, \qquad r^2 = t^2+h^2, \qquad r_1^2 = (s-t)^2, \tag{7}$$
$$r_2^2 = \frac{(ts+h^2-a^2)^2 + h^2(s-t)^2}{s^2+h^2}.$$

For simplicity, σ_{n}^b and σ_{t}^b due to the two edge dislocations can be written in the following forms:

$$\sigma_{\mathrm{n}}^{b}(t,s) = h_{\mathrm{n}1}(t,s)b_x + h_{\mathrm{n}2}(t,s)b_y, \tag{8a}$$

$$\sigma_{\mathrm{t}}^{b}(t,s) = h_{\mathrm{t}1}(t,s)b_x + h_{\mathrm{t}2}(t,s)b_y, \tag{8b}$$

where

$$h_{\mathrm{n}1}(t,s) = h_{xx1}\cos^2\alpha + h_{yy1}\sin^2\alpha + 2h_{xy1}\sin\alpha\cos\alpha, \tag{9a}$$

$$h_{\mathrm{n}2}(t,s) = h_{xx2}\cos^2\alpha + h_{yy2}\sin^2\alpha + 2h_{xy2}\sin\alpha\cos\alpha, \tag{9b}$$

$$h_{\mathrm{t}1}(t,s) = (h_{yy1} - h_{xx1})\sin\alpha\cos\alpha + h_{xy1}(\cos^2\alpha - \sin^2\alpha), \tag{9c}$$

$$h_{\mathrm{t}2}(t,s) = (h_{yy2} - h_{xx2})\sin\alpha\cos\alpha + h_{xy2}(\cos^2\alpha - \sin^2\alpha). \tag{9d}$$

On the other hand, let $\sigma_{\mathrm{n}}^{c}(t)$ and $\sigma_{\mathrm{t}}^{c}(t)$ $(t \in L)$ be the normal and tangential components of the stresses along the line L in Fig. 1(b). According to the solution of Fig. 1(b) given by Xiao and Bai (1999a), we rearrange the coordinate systems adopted in Fig. 2(b) and (c), and a polar coordinate system (r,θ) is introduced. Then, $\sigma_{\mathrm{n}}^{c}(t)$ and $\sigma_{\mathrm{t}}^{c}(t)$ take the form

$$\sigma_{\mathrm{n}}^{c}(t) = \sigma_r^{\mathrm{out}}\cos^2\beta + \sigma_\theta^{\mathrm{out}}\sin^2\beta + 2\sigma_{r\theta}^{\mathrm{out}}\sin\beta\cos\beta = \sigma_{22}^{0}p_1(t), \tag{10a}$$

$$\sigma_{\mathrm{t}}^{c}(t) = (\sigma_\theta^{\mathrm{out}} - \sigma_r^{\mathrm{out}})\sin\beta\cos\beta + \sigma_{r\theta}^{\mathrm{out}}(\cos^2\beta - \sin^2\beta) = \sigma_{22}^{0}p_2(t), \tag{10b}$$

where β is the angle between the n axis and r direction and γ is the angle between the crack line and the x_1 axis. γ is decided by orientation of the crack with respect to the far-field mechanical loading, and

$$\sin\beta = \frac{t}{\sqrt{t^2+h^2}}, \qquad \cos\beta = \frac{h}{\sqrt{t^2+h^2}}, \qquad \theta = \frac{\pi}{2} - \gamma - \beta. \tag{11}$$

The functions $p_1(t)$ and $p_2(t)$ in Eq. (10a) and (10b) take the following form:

$$\begin{aligned} p_1(t) = {} & \frac{1+\cos 2\gamma}{2} + \left(\frac{2v_0-1}{2}\frac{C_{11}^0 + C_{12}^0 - C_{11}^1 - C_{12}^1}{C_{11}^0 - C_{12}^0 + C_{11}^1 + C_{12}^1} \right. \\ & \left. + \frac{2v_0-1}{1-v_0}\frac{C_{11}^0}{C_{11}^0 - C_{12}^0 + C_{11}^1 + C_{12}^1}\frac{e_{13}E_3^0}{\sigma_{22}^0} \right)\frac{a^2}{r^2}\cos 2\beta \\ & + \frac{C_{11}^0 - C_{12}^0 - C_{11}^1 + C_{12}^1}{(6-8v_0)(C_{11}^1 - C_{12}^1) + 2(C_{11}^0 - C_{12}^0)}\left[\left(\frac{2a^2}{r^2} - \frac{3a^4}{r^4} \right)\cos(2\theta - 2\beta) + \frac{2a^2}{r^2}\cos 2\theta \right], \end{aligned} \tag{12a}$$

$$\begin{aligned} p_2(t) = {} & \frac{\sin 2\gamma}{2} + \left(\frac{2v_0-1}{2}\frac{C_{11}^0 + C_{12}^0 - C_{11}^1 - C_{12}^1}{C_{11}^0 - C_{12}^0 + C_{11}^1 + C_{12}^1} \right. \\ & \left. + \frac{2v_0-1}{1-v_0}\frac{C_{11}^0}{C_{11}^0 - C_{12}^0 + C_{11}^1 + C_{12}^1}\frac{e_{13}E_3^0}{\sigma_{22}^0} \right)\frac{a^2}{r^2}\sin 2\beta \\ & - \frac{C_{11}^0 - C_{12}^0 - C_{11}^1 + C_{12}^1}{(6-8v_0)(C_{11}^1 - C_{12}^1) + 2(C_{11}^0 - C_{12}^0)}\left[\left(\frac{2a^2}{r^2} - \frac{3a^4}{r^4} \right)\sin(2\theta - 2\beta) \right] \end{aligned} \tag{12b}$$

in which

$$r = \sqrt{t^2+h^2}. \tag{13}$$

As defined in Fig. 2(b), w is the distance from the center of the crack to n axis. Let B_x and B_y be the dislocation density functions of (s) $(w - c \leqslant s \leqslant w + c)$ along L, using Eqs. (8a), (8b) and (10a), (10b), the stress disturbance problem is thus formulated as

$$-\sigma_{22}^0 p_1(t) = \int_{w-c}^{w+c} [h_{n1}(t,s)B_x(s) + h_{n2}(t,s)B_y(s)]\,\mathrm{d}s, \tag{14a}$$

$$-\sigma_{22}^0 p_2(t) = \int_{w-c}^{w+c} [h_{t1}(t,s)B_x(s) + h_{t2}(t,s)B_y(s)]\,\mathrm{d}s. \tag{14b}$$

The single-value condition of displacement vector requires that the density functions in Eqs. (14a) and (14b) satisfy the following relations:

$$\int_{w-c}^{w+c} B_x(s)\,\mathrm{d}s = 0, \tag{15a}$$

$$\int_{w-c}^{w+c} B_y(s)\,\mathrm{d}s = 0. \tag{15b}$$

The combination of Eqs. (14a), (14b) and (15a), (15b) gives the solution to the problem in Fig. 1(c) for an arbitrarily oriented crack.

3.2. Numerical solution procedures of the integral equations

With the substitution of Eqs. (9a)–(9d) and (7) into Eqs. (14a) and (14b), it is not difficult to show that at $t = s$, the kernels in Eqs. (14a) and (14b) have Cauchy-type singularities. Apart from the singularity terms, all the other terms are bounded in the closed interval $(w - c \leqslant (t,s) \leqslant w + c)$. Separating the singular parts of the kernels, Eqs. (14a), (14b) was rewritten as

$$\begin{aligned}\frac{\pi(k_0+1)}{2G_0}\sigma_{22}^0 p_1(t) = {} & \int_{w-c}^{w+c} B_x(s)\frac{h}{\sqrt{h^2+s}}\frac{\mathrm{d}s}{(s-t)} - \int_{w-c}^{w+c} H_{11}(t,s)B_x(s)\mathrm{d}s \\ & + \int_{w-c}^{w+c} B_y(s)\frac{s}{\sqrt{h^2+s^2}}\frac{\mathrm{d}s}{(s-t)} - \int_{w-c}^{w+c} H_{12}(t,s)B_y(s)\mathrm{d}s,\end{aligned} \tag{16a}$$

$$\begin{aligned}\frac{\pi(k_0+1)}{2G_0}\sigma_{22}^0 p_2(t) = {} & \int_{w-c}^{w+c} B_x(s)\left(-\frac{s}{\sqrt{h^2+s^2}}\frac{\mathrm{d}s}{(s-t)}\right) - \int_{w-c}^{w+c} H_{21}(t,s)B_x(s)\mathrm{d}s \\ & + \int_{w-c}^{w+c} B_y(s)\frac{w}{\sqrt{h^2+s^2}}\frac{\mathrm{d}s}{(s-t)} - \int_{w-c}^{w+c} H_{22}(t,s)B_y(s)\mathrm{d}s,\end{aligned} \tag{16b}$$

where $H_{ij}(t,s)$ $(i,j = 1,2)$ are bounded functions in the closed interval $(w - c \leqslant (t,s) \leqslant w + c)$, and are obtained from Eqs. (14a) and (14b).

Let $t' = (t - w)/c$, $s' = (s - w)/c$, the interval of Eqs. (16a), (16b) can be changed from $(w - c, w + c)$ into $(-1, 1)$ as follows:

$$\begin{aligned}\frac{\pi(k_0+1)}{2G_0}\sigma_{22}^0 p_1'(t') = {} & \int_{-1}^{1} B_x'(s')\frac{h}{\sqrt{h^2+(cs'+w)^2}}\frac{\mathrm{d}s'}{(s'-t')} - \int_{-1}^{1} cH_{11}'(t',s')B_x'(s')\mathrm{d}s' \\ & + \int_{-1}^{1} B_y'(s')\frac{(cs'+w)}{\sqrt{h^2+(cs'+w)^2}}\frac{\mathrm{d}s'}{(s'-t')} - \int_{-1}^{1} cH_{12}'(t',s')B_y'(s')\mathrm{d}s',\end{aligned} \tag{17a}$$

$$\frac{\pi(k_0+1)}{2G_0}\sigma_{22}^0 p_2'(t') = \int_{-1}^{1} B_x'(s')\left(-\frac{(cs'+w)}{\sqrt{h^2+(cs'+w)^2}}\frac{\mathrm{d}s'}{(s'-t')}\right) - \int_{-1}^{1} cH_{21}'(t',s')B_x'(s')\mathrm{d}s' + \int_{-1}^{1} B_y'(s')\frac{h}{\sqrt{h^2+(cs'+w)^2}}\frac{\mathrm{d}s'}{(s'-t')} - \int_{-1}^{1} cH_{22}'(t',s')B_y'(s')\mathrm{d}s', \tag{17b}$$

where $p_1'(t'), p_2'(t'), B_x'(s'), B_y'(s'), H_{ij}'(t',s')$ $(i,j=1,2)$ are, respectively, the corresponding functions of $p_1(t), p_2(t), B_x(s), B_y(s), H_{ij}(t,s)$ $(i,j=1,2)$ in the interval $(-1,1)$. Similarly, Eqs. (15a) and (15b) can be written as:

$$\int_{-1}^{1} B_x'(s')\mathrm{d}s' = 0, \tag{18a}$$

$$\int_{-1}^{1} B_y'(s')\mathrm{d}s' = 0. \tag{18b}$$

As the crack is embedded in the homogeneous isotropic matrix, it is apparent that Eqs. (17a) and (17b) are singular integral equations with an index +1 (Erdogan and Gupta, 1972). Combining with the additional conditions of Eqs. (18a) and (18b), Eqs. (17a) and (17b) can be solved following the Cause–Chebyshev quadrature (Erdogan and Gupta, 1972).

The fundamental function of the system is

$$\omega(s') = (1+s')^{-1/2}(1-s')^{-1/2}. \tag{19}$$

Hence, the solution of Eqs. (17a) and (17b) may be expressed as

$$B_x'(s') = F_1(s')\omega(s'), \tag{20a}$$

$$B_y'(s') = F_2(s')\omega(s'), \tag{20b}$$

where $F_1(s')$,$F_2(s')$ are bounded functions in the interval $(-1,1)$ to be evaluated numerically.

According to the Cause–Chebyshev solution, Eqs. (17a), (17b) and (18a), (18b) can be written in discreet form. As a result a group of $2n$ linear algebra equations with the $2n$ unknowns $F_1(s_k)$ and $F_2(s_k)$ $(k=1,\ldots,n)$ are obtained:

$$\begin{cases} \sum_{k=1}^{n}\frac{1}{n}F_1(s_k)\frac{h}{\sqrt{h^2+(cs_k+w)^2}}\left[\frac{1}{s_k-t_r}-\frac{c\sqrt{h^2+(cs_k+w)^2}}{h}H_{11}'(t_r,s_k)\right] \\ \quad +\sum_{k=1}^{n}\frac{1}{n}F_2(s_k)\frac{(cs_k+w)}{\sqrt{h^2+(cs_k+w)^2}}\left[\frac{1}{s_k-t_r}-\frac{c\sqrt{h^2+(cs_k+w)^2}}{cs_k+w}H_{12}'(t_r,s_k)\right] = \frac{(k_0+1)}{2G_0}\sigma_{22}^0 p_1'(t_r), \\ \sum_{k=1}^{n}\frac{1}{n}F_1(s_k)\frac{(cs_k+w)}{\sqrt{h^2+(cs_k+w)^2}}\left[-\frac{1}{s_k-t_r}-\frac{c\sqrt{h^2+(cs_k+w)^2}}{(cs_k+w)}H_{21}'(t_r,s_k)\right] \\ \quad +\sum_{k=1}^{n}\frac{1}{n}F_2(s_k)\frac{h}{\sqrt{h^2+(cs_k+w)^2}}\left[\frac{1}{s_k-t_r}-\frac{c\sqrt{h^2+(cs_k+w)^2}}{h}H_{22}'(t_r,s_k)\right] = \frac{(k_0+1)}{2G_0}\sigma_{22}^0 p_2'(t_r), \\ \sum_{k=1}^{n}F_1(s_k)=0, \\ \sum_{k=1}^{n}F_2(s_k)=0, \end{cases} \tag{21}$$

where

$$s_k = \cos\frac{(2k-1)\pi}{2n}, \quad k = 1,\ldots,n, \qquad t_r = \cos\frac{\pi r}{n}, \quad r = 1,\ldots,n-1. \tag{22}$$

To simplify the solution procedure, the constant term $((k_0+1)/2G_0)\sigma_{22}^0$ can be removed by defining

$$F_1(s_k) = \frac{(k_0+1)}{2G_0}\sigma_{22}^0 F_1'(s_k), \tag{23a}$$

$$F_2(s_k) = \frac{(k_0+1)}{2G_0}\sigma_{22}^0 F_2'(s_k). \tag{23b}$$

Then Eqs. (21) are thus simplified as

$$\begin{cases} \sum_{k=1}^{n} \frac{1}{n} F_1'(s_k) \frac{h}{\sqrt{h^2+(cs_k+w)^2}} \left[\frac{1}{s_k - t_r} - \frac{c\sqrt{h^2+(cs_k+w)^2}}{h} H_{11}'(t_r, s_k) \right] \\ \quad + \sum_{k=1}^{n} \frac{1}{n} F_2'(s_k) \frac{(cs_k+w)}{\sqrt{h^2+(cs_k+w)^2}} \left[\frac{1}{s_k - t_r} - \frac{c\sqrt{h^2+(cs_k+d)^2}}{cs_k+w} H_{12}'(t_r, s_k) \right] = p_1'(t_r), \\ \sum_{k=1}^{n} \frac{1}{n} F_1'(s_k) \frac{(cs_k+w)}{\sqrt{h^2+(cs_k+w)^2}} \left[-\frac{1}{s_k - t_r} - \frac{c\sqrt{h^2+(cs_k+w)^2}}{(cs_k+w)} H_{21}'(t_r, s_k) \right] \\ \quad + \sum_{k=1}^{n} \frac{1}{n} F_2'(s_k) \frac{h}{\sqrt{h^2+(cs_k+w)^2}} \left[\frac{1}{s_k - t_r} - \frac{c\sqrt{h^2+(cs_k+w)^2}}{h} H_{22}'(t_r, s_k) \right] = p_2'(t_r), \\ \sum_{k=1}^{n} F_1'(s_k) = 0, \\ \sum_{k=1}^{n} F_2'(s_k) = 0. \end{cases} \tag{24}$$

3.3. Stress intensity factor

Following Erdogan et al. (1974), the stress intensity factors at the crack tips can be expressed as

$$K_{\mathrm{I}}(t_1) = -\frac{2G_0}{1+k_0}\frac{\sqrt{c}}{\sqrt{h^2+(w-c)^2}}[hF_1(-1) + (w-c)F_2(-1)], \tag{25a}$$

$$K_{\mathrm{II}}(t_1) = -\frac{2G_0}{1+k_0}\frac{\sqrt{c}}{\sqrt{h^2+(w-c)^2}}[(w-c)F_1(-1) - hF_2(-1)], \tag{25b}$$

$$K_{\mathrm{I}}(t_2) = \frac{2G_0}{1+k_0}\frac{\sqrt{c}}{\sqrt{h^2+(w+c)^2}}[hF_1(1) + (w+c)F_2(1)], \tag{25c}$$

$$K_{\mathrm{II}}(t_2) = \frac{2G_0}{1+k_0}\frac{\sqrt{c}}{\sqrt{h^2+(w+c)^2}}[(w+c)F_1(1) - hF_2(1)] \tag{25d}$$

where K_{I} and K_{II} are the Mode I and Mode II stress intensity factors of the crack, respectively. t_1 and t_2 refer to the two crack tips, and $t_1 < t_2$ in the (t, n) coordinate system. With the substitution of Eqs. (23a) and (23b) into Eqs. (25a)–(25d), the stress intensity factor can be expressed as

$$K_{\mathrm{I}}(t_1) = -\sigma_{22}^0 \frac{\sqrt{c}}{\sqrt{h^2 + (w-c)^2}} [hF_1'(-1) + (w-c)F_2'(-1)], \tag{26a}$$

$$K_{\mathrm{II}}(t_1) = -\sigma_{22}^0 \frac{\sqrt{c}}{\sqrt{h^2 + (w-c)^2}} [(w-c)F_1'(-1) - hF_2'(-1)], \tag{26b}$$

$$K_{\mathrm{I}}(t_2) = \sigma_{22}^0 \frac{\sqrt{c}}{\sqrt{h^2 + (w+c)^2}} [hF_1'(1) + (w+c)F_2'(1)], \tag{26c}$$

$$K_{\mathrm{II}}(t_2) = \sigma_{22}^0 \frac{\sqrt{c}}{\sqrt{h^2 + (w+c)^2}} [(w+c)F_1'(1) - hF_2'(1)]. \tag{26d}$$

$F_1'(1), F_1'(-1), F_2'(1), F_2'(-1)$ are solved from equation group (24). If the stress intensity factors are normalized by

$$K_{\mathrm{I}}^0 = \sigma_{22}^0 \sqrt{c}, \tag{27}$$

which is the stress intensity factor for a uniaxially stressed infinite plane containing a crack of length $2c$ perpendicular to the direction of loading, then it comes that

$$\frac{K_{\mathrm{I}}(t_1)}{K_{\mathrm{I}}^0} = -\frac{(w-c)F_2'(-1) + hF_1'(-1)}{\sqrt{h^2 + (w-c)^2}}, \tag{28a}$$

$$\frac{K_{\mathrm{II}}(t_1)}{K_{\mathrm{I}}^0} = -\frac{(w-c)F_1'(-1) - hF_2'(-1)}{\sqrt{h^2 + (w-c)^2}}, \tag{28b}$$

$$\frac{K_{\mathrm{I}}(t_2)}{K_{\mathrm{I}}^0} = \frac{(w+c)F_2'(1) + hF_1'(1)}{\sqrt{h^2 + (w+c)^2}}, \tag{28c}$$

$$\frac{K_{\mathrm{II}}(t_2)}{K_{\mathrm{I}}^0} = \frac{(w+c)F_1'(1) - hF_2'(1)}{\sqrt{h^2 + (w+c)^2}}. \tag{28d}$$

From the structure of the equation group (24) and the normalized stress intensity factor expressed in Eqs. (28a)–(28d), it can be seen apparently that the stress intensity factors at crack tips are influenced by the far-field electro-mechanical loading, material properties of the piezoelectric inhomogeneity and the crack, and the inhomogeneity–crack geometric configuration, etc. In order to understand these influences in detail, numerical examples are given in the following section under various parameters and geometric configurations.

One thing that should be mentioned here is that in Fig. 2, for the basic solution of edge dislocation–inhomogeneity interaction used, the inhomogeneity should be made of conventional pure elastic material, instead of piezoelectric material. As a result, the integral Eqs. (14a) and (14b) based on the single dislocation solution are approximately correct. However, our FEM results show that the error caused is less than 1%. The reason that the error caused by this approximation is very small can be analyzed as follows: after the superposition process in Fig. 1, there is no electrical loading in Fig. 1(c). Only the mechanical traction along the two crack faces in Fig. 1(c) will cause piezoelectric effect on the inhomogeneity. This

piezoelectric effect will influence the stress field inside the inhomogeneity, thus conversely cause the change of the stress field near the crack tip. However, this feedback effect is two orders lower than the external applied loading.

4. Numerical examples and FEM confirmations

It is evident that the stress intensity factors (SIFs) associated with Fig. 1(c) are also the SIFs for the problem of Fig. 1(a). In this section, the numerical examples of the SIFs under different influence parameters in three geometric crack–inhomogeneity configurations are presented, and the influence of the inhomogeneity on the SIF of the crack is discussed. As the derivations are so tedious, it is easy to make mistakes during the derivation procedures; hence, an independent finite element analysis is performed to check the results obtained. The finite element program employed is ANSYS version 5.4 (1995).

For both the finite element analysis and numerical examples, the crack length $2c$ is set to be one-half of the radius of the inhomogeneity, i.e. $c = a/4$. The inhomogeneity is made of PZT-5H. The values of material constants for PZT-5H are listed in Table 1. Poisson's ratio of the matrix is assumed to be $v_0 = 1/3$. The far-field in-plane uniaxial tension σ_{22}^0 is used as a normalizing parameter.

The variation ranges of the main influence factors on the SIFs of the crack are selected based on practical applications of piezoelectric sensor. $e_{13}E_3^0/\sigma_{22}^0$ is taken as the normalized far-field electric loading. Since the piezoelectric constants e_{13} is negative, $e_{13}E_3^0/\sigma_{22}^0 < 0$ represents the case that the far electric field E_3^0 is along the x_3 axis, while $e_{13}E_3^0/\sigma_{22}^0 > 0$ is the case that E_3^0 is in the opposite direction of x_3 axis. G_0 and G_1 are shear moduli of the matrix and the piezoelectric sensor, respectively. As defined in Eqs. (4), parameter $m = G_1/G_0$ represents the shear modulus ratio of the piezoelectric inhomogeneity to the matrix. $m = 0.1$ represents the case that the matrix is "harder" than the piezoelectric sensor; $m = 10.0$ is the case that the matrix is "softer" than the sensor.

In the finite element analysis, the problem in Fig. 1 is solved directly without the superposition process. Due to the far-field electric loading along the x_3 axis, 3-D finite element analysis is employed. The plain strain condition is achieved by constraining the UZ degree of freedom (displacement in the Z-direction) of all nodes. The uniform far-field electric loading is applied by constraining the VOLT degree of freedom of the nodes on the front plane by V_1 and that on the back plane by V_2. The electric field is thus obtained as $E_3^0 = (V_1 - V_2)/T$, in which T is the thickness of the model along the Z-direction. The 3-D coupled-field SOLID 5 is used to model the piezoelectric inhomogeneity and the 3-D structural SOLID 45 is used for the surrounding elastic matrix. The macro FRACT is used to create SOLID 95 crack tip element from the SOLID 45 model using a weighted midside node position (quarter point location). SOLID 95 is the 20-node brick element for crack tip mesh. The first row of elements around the crack front are singular elements. For each geometric configuration, a corresponding finite element model is built with different numbers of elements and nodes. The KCALC command in POST1 is used to get the SIFs by displacement extrapolation.

4.1. Crack–inhomogeneity interaction configuration I

The first configuration considered is shown in Fig. 3, the crack is perpendicular to the far-field mechanical loading and is situated near the inhomogeneity, with the crack face and the center of the

Table 1
Material constants of a piezoelectric material C_{ij} (10^{10} N/m^2), e_{kl} (C/m^2), ε_{11} (10^{-10} C/V$_m$)

	C_{11}	C_{33}	C_{44}	C_{12}	C_{13}	e_{13}	e_{33}	e_{15}	ε_{11}	ε_{33}
PZT-5H	12.6	11.7	3.53	5.5	5.3	−6.5	23.3	17.0	151	130

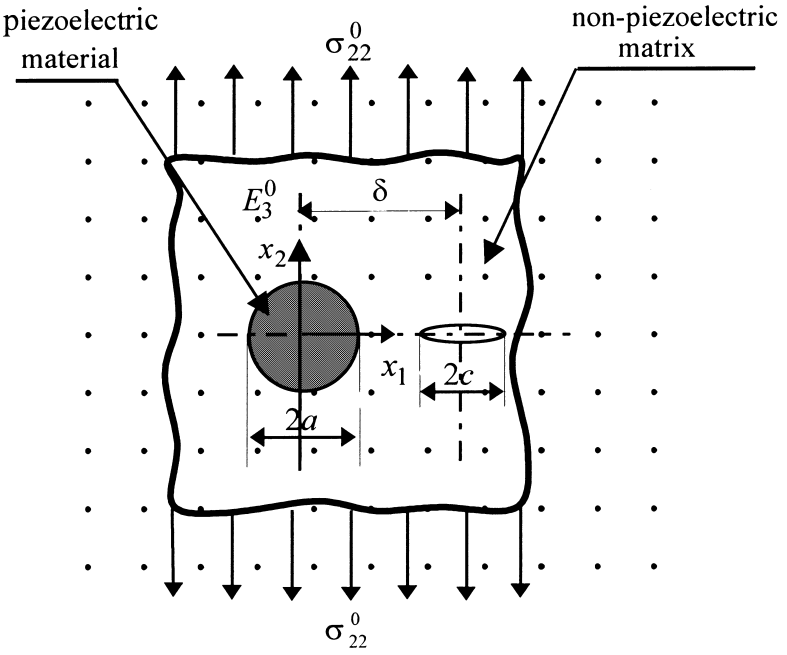

Fig. 3. Crack–inhomogeneity interaction configuration I.

inhomogeneity being in the same line, i.e. $\gamma = 0^\circ$ in Fig. 2(c) and $\lambda = 0^\circ$ in Fig. 2(b). The distance between the centers of the crack and the inhomogeneity is denoted by δ.

According to the crack orientation, the SIFs can be evaluated directly following the derivation procedure (Eqs. (1)–(28)). For the present configuration, parameters defined in Fig. 2 are as follows:

$$\lambda = 0, \quad \gamma = 0, \quad h = 0, \quad w = \delta, \quad c = a/4. \tag{29}$$

Only normal stress exists on the crack surfaces for this configuration, so only the edge dislocation with Burger's vector b_y is involved. With the substitution of above parameters into Eqs. (1)–(17), the integral equation is obtained as

$$\int_{-1}^{1} \left[\frac{1}{\pi} \frac{1}{t' - s'} + \phi(t', s') \right] B_y'(s')\, \mathrm{d}s' = -\frac{(1 + k_0)}{2G_0} \sigma_\theta^{\text{out}}, \tag{30}$$

where

$$\phi(t', s') = \frac{1}{4\pi} \left\{ -(A + B) \frac{1}{2(\frac{\delta}{a} + \frac{t'}{4})[(\frac{\delta}{a} + \frac{t'}{4})(\frac{\delta}{a} + \frac{s'}{4}) - 1]} - A \frac{\beta^2 - 1}{\beta^3} \left[\beta^2 - \frac{\beta^2 - 1}{\beta} \frac{(\frac{\delta}{a} + \frac{s'}{4})}{(\frac{\delta}{a} + \frac{s'}{4})(\frac{\delta}{a} + \frac{t'}{4}) - 1} \right] \right.$$
$$\left. \times \frac{a^2 (\frac{\delta}{a} + \frac{s'}{4})^2}{[(\frac{\delta}{a} + \frac{s'}{4})(\frac{\delta}{a} + \frac{t'}{4}) - 1]^2} + A \frac{1}{(\frac{\delta}{a} + \frac{t'}{4})^3} + \frac{1}{2\beta} \frac{1}{(\frac{\delta}{a} + \frac{t'}{4})^2} [A(2\beta^2 - 1) + M(1 + k_1) - 1] \right\} \tag{31}$$

and

$$\sigma_\theta^{\text{out}}(t') = \sigma_{22}^0 \left\{ 1 + \frac{1}{2} \left[\left(\frac{G_0 - \frac{1-2\nu_0}{1-2\nu_1} G_1}{G_0 + \frac{G_1}{1-2\nu_1}} + \frac{2G_0}{G_0 + \frac{G_1}{1-2\nu_1}} \frac{e_{13} E_3^0}{\sigma_{22}^0} \right) \frac{1}{\left(\frac{\delta}{a} + \frac{t'}{4}\right)^2} + \frac{G_0 - G_1}{G_0 + (3-4\nu_0) G_1} \frac{3}{\left(\frac{\delta}{a} + \frac{t'}{4}\right)^4} \right] \right\}. \tag{32}$$

The expression of $\sigma_\theta^{\text{out}}(t')$ is from Xiao and Bai (1999a) in terms of variable (t') and material constants G_0, G_1, ν_0, ν_1. According to Eqs. (18a) and (18b), the additional condition for the dislocation density function $B_y'(s')$ is

$$\int_{-1}^{1} B_y'(s')\,\mathrm{d}s' = 0. \tag{33}$$

Eq. (31) can be solved in a straightforward manner with the numerical technique explained in Eqs. (19)–(24). The numerical solution of Eq. (30) is denoted by $F_2(s')$. However, to reduce the parameters involved in the solution procedure, some simplifications can be made. By analyzing the structure of the expression $\sigma_\theta^{\text{out}}(t')$ in Eq. (32), it is observed that $\sigma_\theta^{\text{out}}(t')$is the linear function of the terms $1/(\delta/a + t'/4)^2$ and $1/(\delta/a + t'/4)^4$ with constant coefficients. Denoting $P_1(s')$, $P_2(s')$, $P_3(s')$ as the solution from the following three sets of linear system, the solution $F_2(s')$ can be obtained as the linear combination of $P_1(s')$, $P_2(s')$, $P_3(s')$:

$$\begin{cases} \sum_{k=1}^{n} \frac{1}{n} P_1(s_k) \left[\frac{1}{t_r - s_k} + \pi \phi(t_r, s_k) \right] = 1, \\ \sum_{k=1}^{n} P_1(s_k) = 0, \end{cases} \tag{34a}$$

$$\begin{cases} \sum_{k=1}^{n} \frac{1}{n} P_2(s_k) \left[\frac{1}{t_r - s_k} + \pi \phi(t_r, s_k) \right] = \frac{1}{\left(\frac{t_r}{4} + \frac{\delta}{a}\right)^2}, \\ \sum_{k=1}^{n} P_2(s_k) = 0, \end{cases} \tag{34b}$$

and

$$\begin{cases} \sum_{k=1}^{n} \frac{1}{n} P_3(t_k) \left[\frac{1}{t_r - s_k} + \pi \phi(t_r, s_k) \right] = \frac{1}{\left(\frac{t_r}{4} + \frac{\delta}{a}\right)^4}, \\ \sum_{k=1}^{n} P_3(s_k) = 0. \end{cases} \tag{34c}$$

Then, $F_2(s')$ is evaluated through

$$F_2(s') = -\frac{(1+k_0)}{2G_0} \sigma_{22}^0 \left\{ P_1(s') + \frac{1}{2} \left[\left(\frac{G_0 - \frac{1-2\nu_0}{1-2\nu_1} G_1}{G_0 + \frac{G_1}{1-2\nu_1}} + \frac{2G_0}{G_0 + \frac{G_1}{1-2\nu_1}} \frac{e_{13} E_3^0}{\sigma_{22}^0} \right) P_2(s') + \frac{3(G_0 - G_1)}{G_0 + (3-4\nu_0) G_1} P_3(s') \right] \right\}. \tag{35}$$

Following Eqs. (25)–(28), the normalized Mode I SIFs at both crack tips can be expressed as

$$\frac{K_{\text{I}}(t_1)}{K_{\text{I}}^0} = P_1(-1) + \frac{1}{2} \left[\frac{G_0 - \frac{1-2\nu_0}{1-2\nu_1} G_1}{G_0 + \frac{G_1}{1-2\nu_1}} P_2(-1) + \frac{3(G_0 - G_1)}{G_0 + (3-4\nu_0) G_1} P_3(-1) \right] + \frac{G_0 P_2(-1)}{G_0 + \frac{G_1}{1-2\nu_1}} \frac{e_{13} E_3^0}{\sigma_{22}^0}, \tag{36a}$$

$$\frac{K_{\mathrm{I}}(t_2)}{K_{\mathrm{I}}^0} = P_1(1) + \frac{1}{2}\left[\frac{G_0 - \frac{1-2\nu_0}{1-2\nu_1}G_1}{G_0 + \frac{G_1}{1-2\nu_1}}P_2(1) + \frac{3(G_0 - G_1)}{G_0 + (3-4\nu_0)G_1}P_3(1)\right] + \frac{G_0 P_2(1)}{G_0 + \frac{G_1}{1-2\nu_1}}\frac{e_{13}E_3^0}{\sigma_{22}^0}. \tag{36b}$$

It is noted that $P_1(\pm 1)$, $P_2(\pm 1)$ and $P_3(\pm 1)$ solved from Eqs. (34a)–(34c) are related to the normalized distance δ/a and material constants in $\phi(s', t')$. The above expressions show that the normalized far-field electric loading $e_{13}E_3^0/\sigma_{22}^0$ has linear influence on the SIFs at crack tips. This is true with the crack in any other orientations outside the inhomogeneity. The reason is that the inhomogeneity is made of linear piezoelectric material and the stress field outside the inhomogeneity is linearly related to $e_{13}E_3^0/\sigma_{22}^0$.

Finite element computation is performed to check the possible errors made due to the tedious derivations. A half model is used because of the symmetry about the x_1 axis. The mesh of the model is illustrated in Fig. 4, where Fig. 4(a) is the overall 3-D mesh of the model, Fig. 4(b) is a plane view of the mesh near the inhomogeneity–crack area, and Fig. 4(c) is the mesh near the crack tip. The length of the element at the crack front is taken as $0.05c$. For the current configuration only Mode I stress intensity factor K_{I} exists. Comparisons are made between the normalized SIFs $K_{\mathrm{I}}/K_{\mathrm{I}}^0$ obtained from the distributed dislocation technique and FEM, under two sets of material constants combinations as shown in Fig. 5(a) and (b), where the far-field electric loading is taken to be the same, i.e. $e_{13}E_3^0/\sigma_{22}^0 = 0.1$, and the shear modulus ratio of the inhomogeneity to the matrix is taken as $m = 10.0$ and $m = 0.1$, respectively. It is shown that results obtained through the distributed dislocation theory coincide well with the finite element analysis.

After the FEM verification, some other numerical calculations involving different parameters are also performed based purely on the solution procedure described in Eqs. (32)–(36). Due to electro-mechanical coupling behavior of the piezoelectric material, interaction between the piezoelectric inhomogeneity and the crack is greatly affected by the far-field electric loading. As mentioned above, for the linear piezoelectric material, the influence of the electric loading on the SIF is linear. When the crack almost touches the piezoelectric inhomogeneity, the interaction between them becomes the largest. Fig. 6 shows the variation of $K_{\mathrm{I}}/K_{\mathrm{I}}^0$ at the two crack tips with the normalized far-field electric loading $e_{13}E_3^0/\sigma_{22}^0$ when $\delta = a + c + 0.01a$, i.e. the distance between the left crack tip and the inhomogeneity is only 0.01a. It can be seen that when the matrix is "harder" than the piezoelectric inhomogeneity (Fig. 6(a)), the influence of the far electric field on the SIF of the left crack tip is much greater than that on the right tip. In this case, the SIFs on both tips are much bigger than K_{I}^0 (The SIF of the crack without the inhomogeneity, as given in Eq. (27)), and the left tip is more dangerous than the right one. On the contrary, when the matrix is "softer" than the inhomogeneity (Fig. 6(b)), the SIFs K_{I} at both tips of the crack are smaller than K_{I}^0, and the left tip is safer than the right tip. So the left tip of the crack undergoes the greatest increase or decrease with the variation of E_3^0 and the inhomogeneity–matrix elastic modulus ratio. This is logical since the influence of the piezoelectric inhomogeneity will be more pronounced to the nearer crack tip.

Fig. 6 indicates that the SIF tends to be infinitely large when the normalized electric loading $e_{13}E_3^0/\sigma_{22}^0$ increases along the positive x_3 direction. In other words, the crack is very dangerous when E_3^0 increases along the opposite x_3 axis direction (please note e_{13} is negative). On the other hand, the crack propagation can be arrested if we increase E_3^0 along the positive x_3 axis direction. In Fig. 7, the interaction between the crack and the inhomogeneity is considered for E_3^0 in the opposite x_3 direction for different modulus ratios. When E_3^0 is strong in the opposite x_3 direction, the variation of $K_{\mathrm{I}}/K_{\mathrm{I}}^0$ with the normalized distance δ/a is large. But with increasing distances, the SIF of the crack tends to be constant at 1.0 in any case.

According to the numerical examples, we can see that the electric field plays an important role in the interaction between the piezoelectric inhomogeneity and the crack. It has a linear relationship to the SIFs of the crack. But the variation of the SIFs with the electric field is greatly affected by the direction of the electric field. Only when the far electric field E_3^0 increases along a certain direction, the SIF increases. The extent of the influence of the electric field is decided by the distance between the crack and the inhomo-

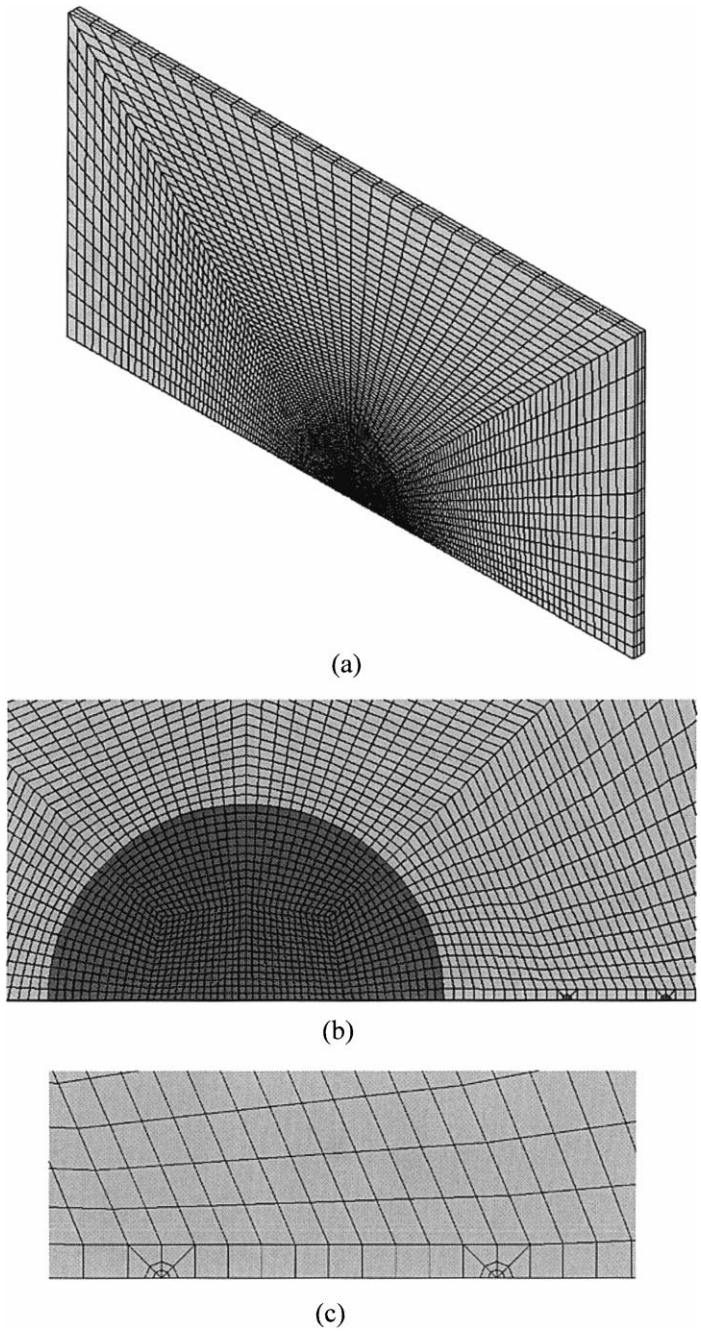

Fig. 4. The finite element model in the case of $\lambda = 0°$: (a) the overall 3-D mesh; (b) the mesh near the inhomogeneity and crack area and (c) the magnified mesh figure near crack tips.

geneity, as well as the material properties of the matrix and the inhomogeneity. When the electric loading is much weaker than the mechanical loading, i.e. the mechanical loading is dominant, the influence of the piezoelectric inhomogeneity on the crack is similar to that of an elastic inhomogeneity on a crack.

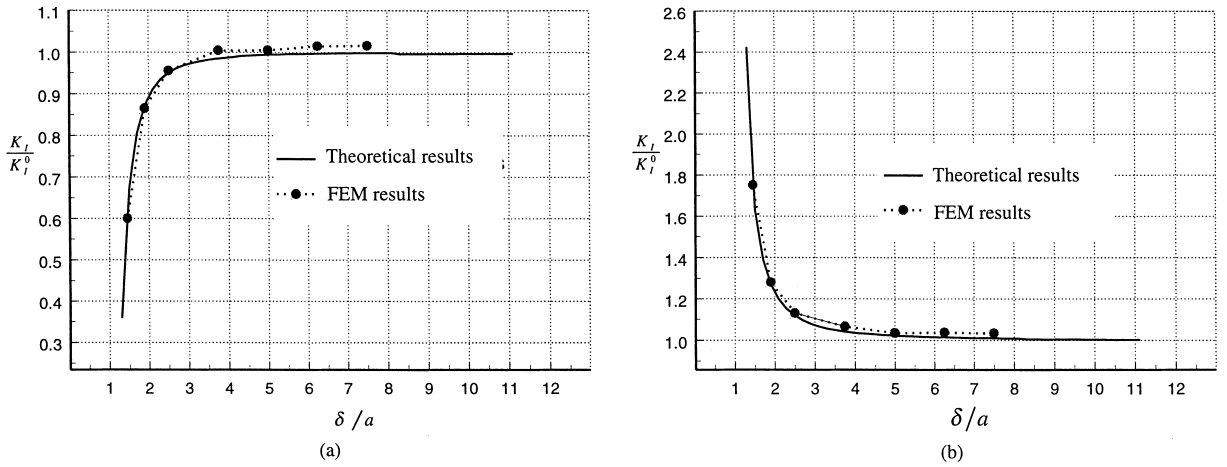

Fig. 5. Verification of SIF by FEM analysis in the case of $\lambda = 0°$ under different material constant ratio: (a) $e_{13}E_3^0/\sigma_{22}^0 = 0.1,\ m = 10.0$ and (b) $e_{13}E_3^0/\sigma_{22}^0 = 0.1,\ m = 0.1$.

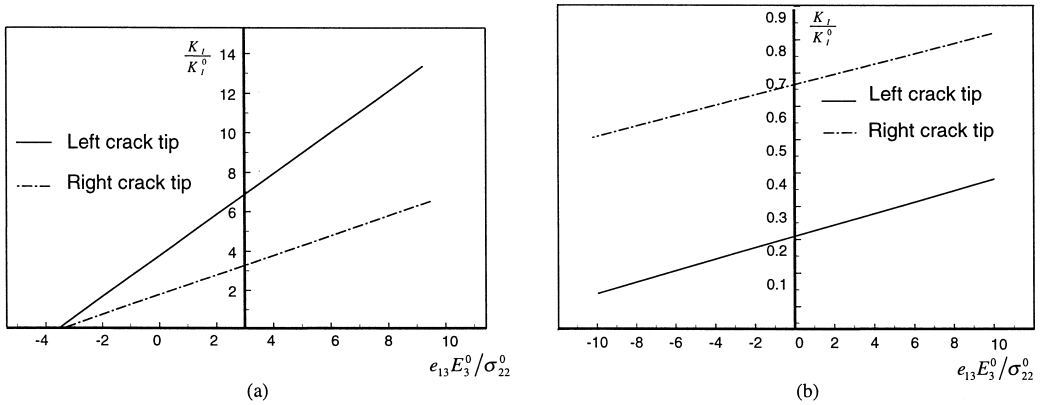

Fig. 6. The SIFs at both crack tips when the crack almost touches the piezoelectric inhomogeneity ($\delta = a + c + 0.01a$) under different elastic modulus ratio: (a) $m = 10.0$ and (b) $m = 0.1$.

4.2. Crack–inhomogeneity interaction configuration II

The second configuration considered is shown in Fig. 8, where the crack face is perpendicular to the far-field mechanical loading and it is directly above the inhomogeneity, with the connection line between the centers of the crack and the inhomogeneity being perpendicular to the crack face, i.e. $\gamma = 0°$ in Fig. 2(c) and $\lambda = 90°$ in Fig. 2(b). Other parameters defined in Fig. 2 are as follows:

$$h = \delta, \quad w = 0, \quad c = a/4. \tag{37}$$

With the substitution of these parameters into the derivation procedure (Eqs. (1)–(28)), equations similar to Eqs. (36a) and (36b) on the SIFs at the two crack tips can be obtained. Since the formulation procedure is similar and parallel to that of Configuration I described in the previous sub-section, here we present only the numerical results and omit the detailed equation.

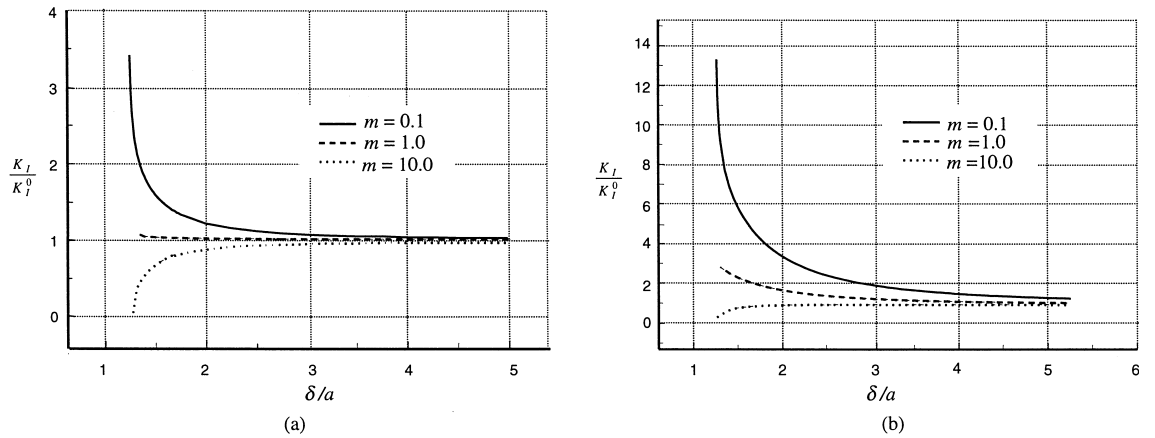

Fig. 7. Variation of K_I/K_I^0 with δ/a when $\lambda = 0°$ under different far field electric loading: (a) $e_{13}E_3^0/\sigma_{22}^0 = 0.1$; (b) $e_{13}E_3^0/\sigma_{22}^0 = 10.0$.

FEM analysis is again performed to check possible errors made due to the tedious derivations. A half-model is used as the problem is symmetric about x_2 axis. The mesh of the model is illustrated in Fig. 9, where Fig. 9(a) is the overall 3-D mesh of the model, Fig. 9(b) is a plane view of the mesh near the inhomogeneity–crack area, and Fig. 9(c) is the mesh near crack tips. The length of the element at the crack front is taken as $c/8$. For this configuration, both Mode I and Mode II stress intensity factors exist.

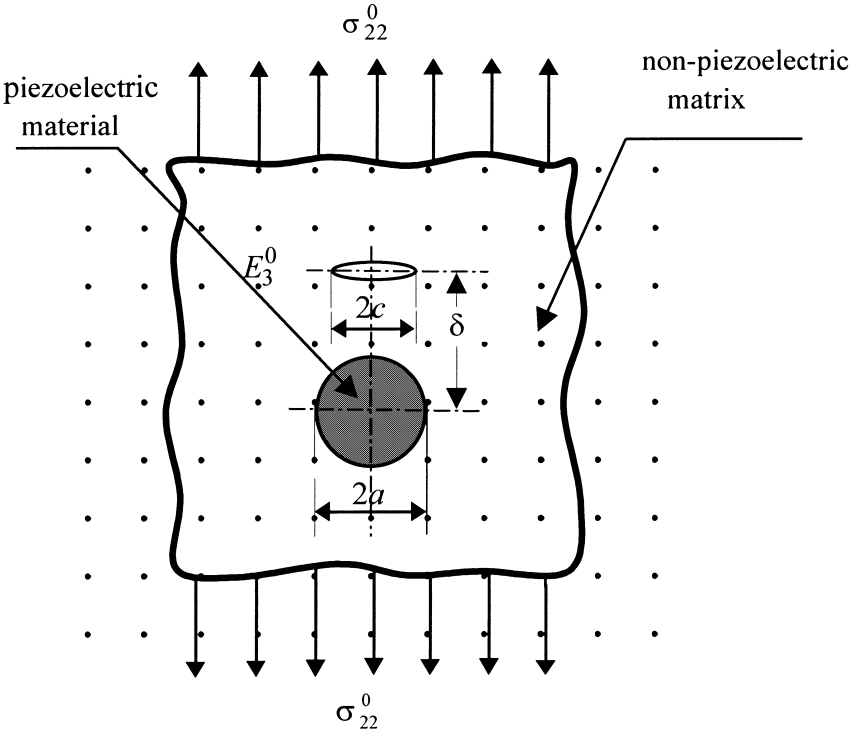

Fig. 8. Crack–inhomogeneity interaction configuration II.

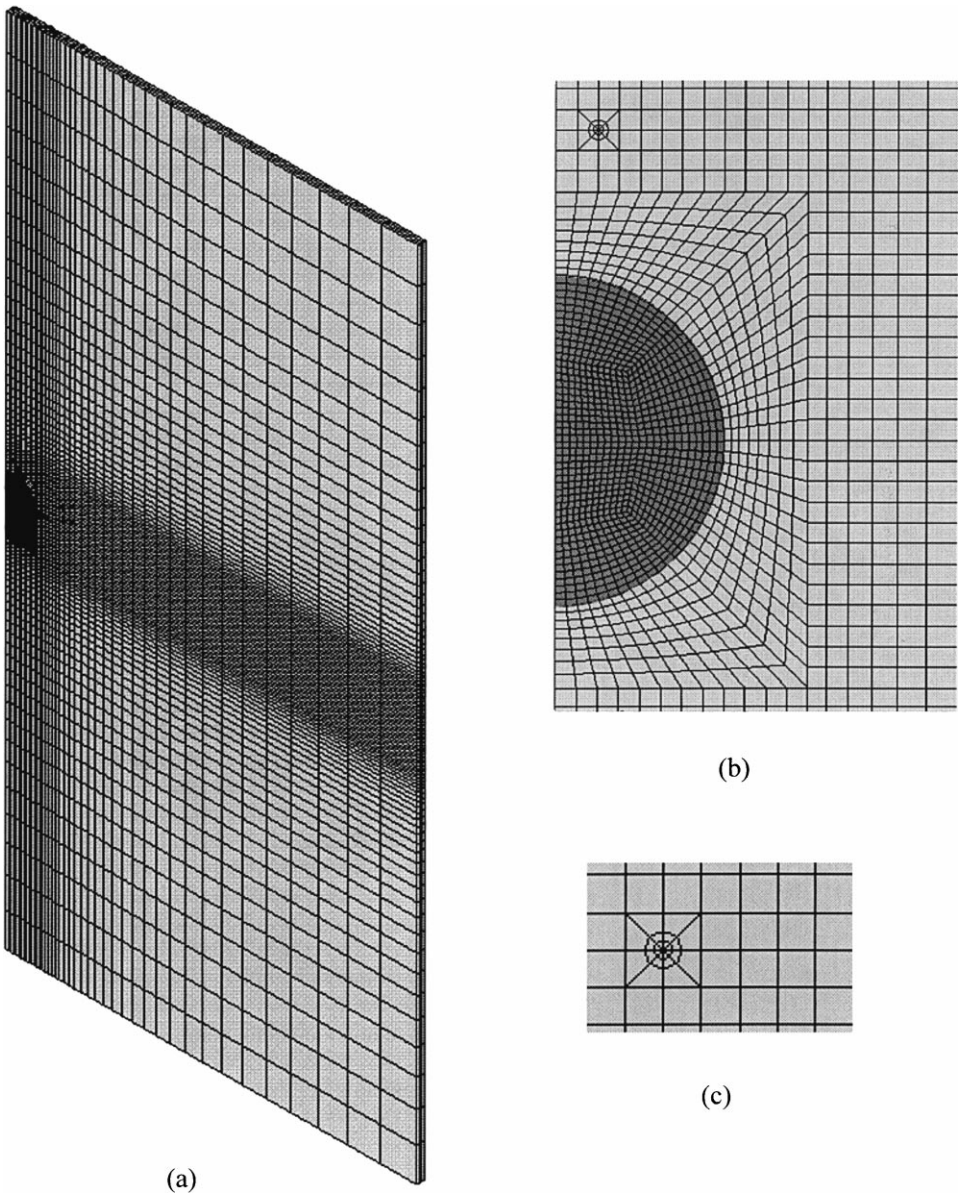

Fig. 9. Finite element model in the case of $\lambda = 90°$: (a) the overall 3-D mesh; (b) the mesh near inhomogeneity–crack area and (c) the magnified mesh figure near the crack tip.

Comparisons are made between the normalized SIFs obtained from the distributed dislocation technique and FEM under two different conditions. The verification results of K_I/K_I^0 and K_{II}/K_I^0 is presented in Figs. 10 and 11, respectively. From the verification results, it can be concluded that results obtained through distributed dislocation theory coincide well with finite element analysis.

The present configuration involves both Mode I and Mode II stress intensity factors. Fig. 12 shows the comparison of K_I and K_{II} at the crack tip. It can be seen that the changing tendency of K_{II} with the external

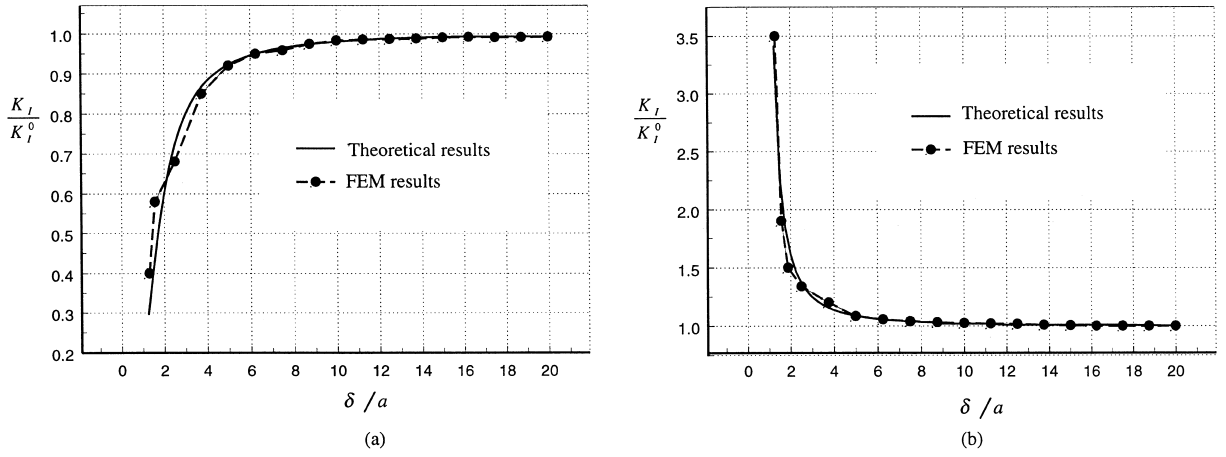

Fig. 10. Verification of K_{I} for $\lambda = 90°$: (a) $e_{13}E_3^0/\sigma_{22}^0 = 0.1,\ m = 0.1$ and (b) $e_{13}E_3^0/\sigma_{22}^0 = -5.0,\ m = 0.1$.

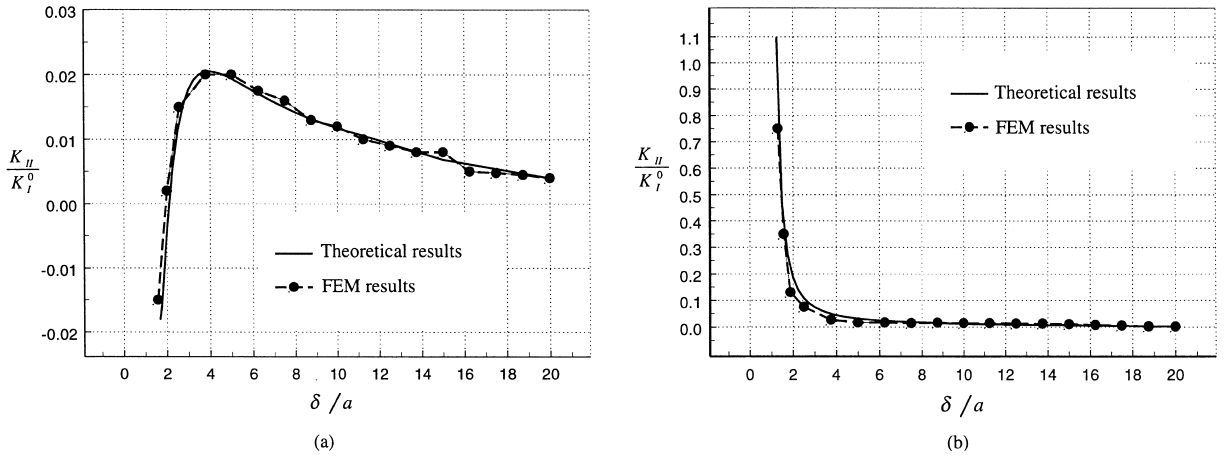

Fig. 11. Verification of K_{II} for $\lambda = 90°$: (a) $e_{13}E_3^0/\sigma_{22}^0 = 0.1,\ m = 0.1$ and (b) $e_{13}E_3^0/\sigma_{22}^0 = -5.0,\ m = 0.1$.

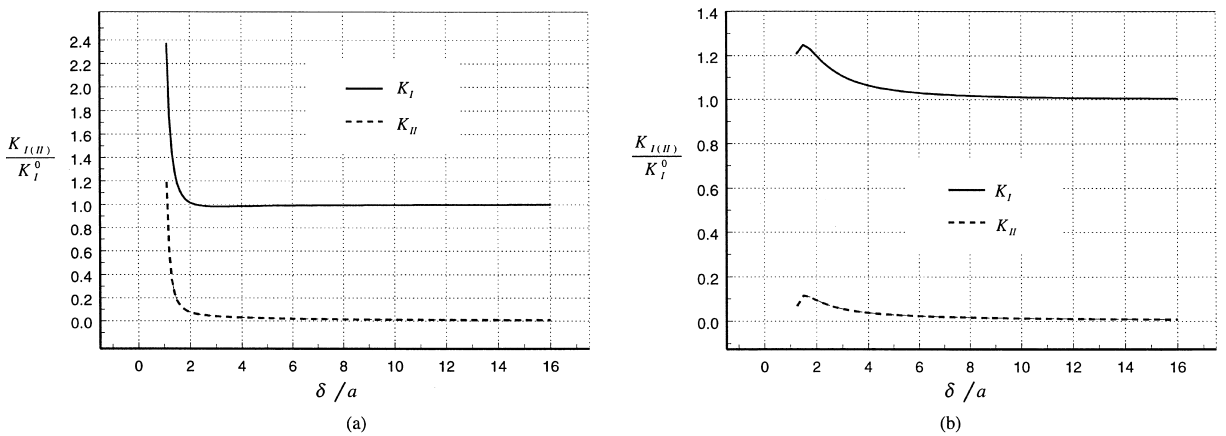

Fig. 12. Comparison of K_{I} and K_{II} for $\lambda = 90°$: (a) $e_{13}E_3^0/\sigma_{22}^0 = -2.0,\ m = 0.1$ and (b) $e_{13}E_3^0/\sigma_{22}^0 = 2.0,\ m = 10.0$.

conditions is very similar to that of K_I. It also shows that K_{II} is much smaller than K_I and tends to be zero with an increase in distance δ. This phenomenon is evident, as the applied loading is perpendicular to the crack face. The following analysis will focus on the Mode I stress intensity factor.

Due to the electro-mechanical coupling behavior of the piezoelectric material, interaction between the inhomogeneity and the crack is greatly affected by the far-field electric loading. Fig. 13 shows the variation of the normalized SIF K_I/K_I^0 with the normalized distance δ/a under the conditions $e_{13}E_3^0/\sigma_{22}^0 = 2.0$ and $e_{13}E_3^0/\sigma_{22}^0 = -2.0$, respectively. A comparison of Fig. 13(a) and (b) shows that the SIF of the crack is much smaller at positive $e_{13}E_3^0/\sigma_{22}^0$ value than that at negative $e_{13}E_3^0/\sigma_{22}^0$ value. Since K_I/K_I^0 is linearly related to the far-field electric loading for linear piezoelectric inhomogeneity, the SIF of the crack will increase linearly when the far electric field E_3^0 increases along the positive x_3 direction (as e_{13} is negative), which is in contrast to the case shown in Fig. 6. So, E_3^0 along the opposite x_3 direction can protect the crack from propagation for the current configuration.

The distance δ between the inhomogeneity and the crack is also a main factor to influence the SIF of the crack. The effect of the inhomogeneity to the crack weakens as δ increases. The normalized SIF K_I/K_I^0 tends to be 1.0 when δ goes to infinity. This means that the interaction between the crack and the inhomogeneity ceases after some distance.

Apart from the influence of the far-field electric loading and the distance δ, the SIF is also related to the materials properties. When $m = 0.1$ and δ/a is in small value, K_I/K_I^0 increases sharply with δ/a as shown in Fig. 13(a), whereas it drops quickly with δ/a in Fig. 13(b) for reversed electric loading. This can demonstrate that the interaction between the crack and the piezoelectric inhomogeneity responds sensitively to the varying external conditions when the piezoelectric inhomogeneity is "softer" than the matrix. When $m = 10.0$, K_I/K_I^0 varies marginally with the increasing δ/a. In other words, the variation of K_I/K_I^0 with δ/a is not that sensitive to electric loading when the inhomogeneity is "harder" than the matrix. However, Fig. 13 also indicates that for $m = 10.0$, the Mode I SIF K_I is always higher than K_I^0, which means a "harder" inhomogeneity makes the crack easier to propagate for this configuration.

4.3. Crack–inhomogeneity interaction configuration III

The third configuration studied is shown in Fig. 14, the crack is perpendicular to the far-field mechanical loading and it is located at an oblique angle 45° with reference to the connection line between the centers of the crack and the inhomogeneity. For the present configuration, parameters defined in Fig. 2 are as follows:

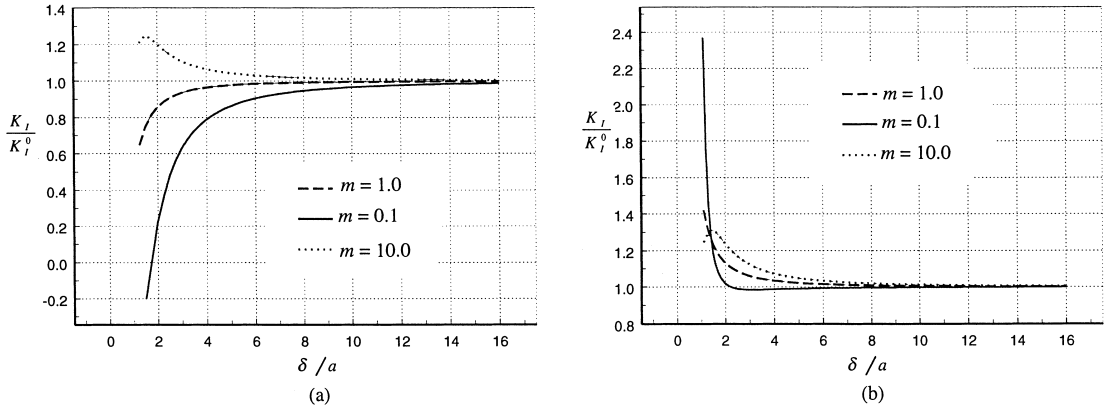

Fig. 13. Variation of K_I with δ when $\lambda = 90°$: (a) $e_{13}E_3^0/\sigma_{22}^0 = 2.0$ and (b) $e_{13}E_3^0/\sigma_{22}^0 = -2.0$.

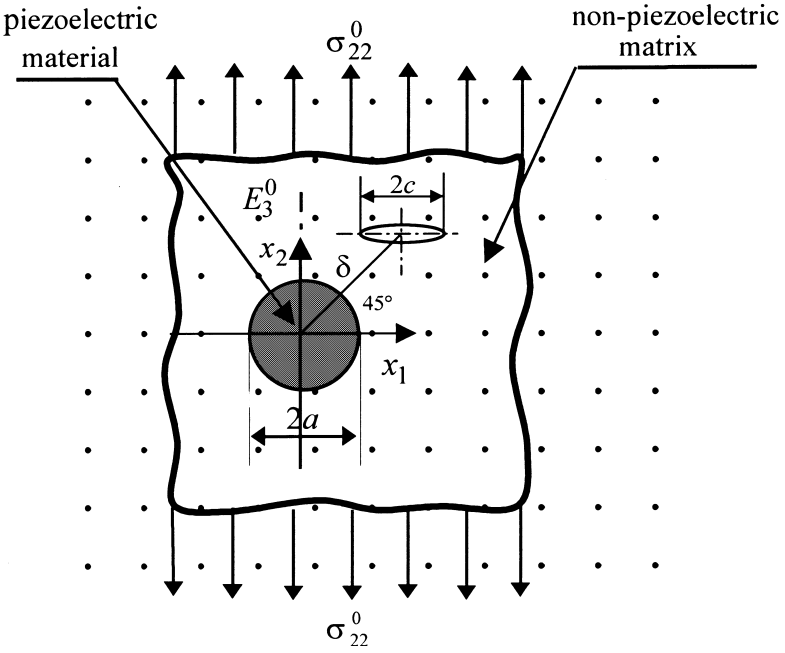

Fig. 14. Crack–inhomogeneity interaction configuration III.

$$\lambda = 45^\circ, \quad \gamma = 0, \quad h = \delta/\sqrt{2}, \quad w = \delta/\sqrt{2}, \quad c = a/4. \tag{38}$$

With the substitution of these parameters into Eqs. (1)–(28), by procedures similar to the previous two subsections, numerical results for the SIFs are obtained parallel.

FEM analysis is performed again to check the tedious derivations. A full model is employed for the finite element analysis. The mesh of the model is illustrated in Fig. 15, where Fig. 15(a) is the overall 3-D mesh of the model, Fig. 15(b) is a plane view of the mesh near the piezoelectric-crack area and Fig. 15(c) is the mesh near the crack tip. The length of the element at the crack front is taken as $c/8$. For this configuration, both Mode I and Mode II stress intensity factors exist. Comparisons are made between the normalized SIFs obtained from the distributed dislocation technique and FEM under two sets of parameters. The verification results of K_I/K_I^0 and K_{II}/K_I^0 is presented in Figs. 16 and 17, respectively. It is clear that results obtained through distributed dislocation theory coincide well with finite element analysis.

The present configuration involves both Mode I and Mode II SIFs, and the values at the two crack tips are different. The difference of the SIFs at the two crack tips is shown in Fig. 18, where Fig. 18(a) refers to K_I and Fig. 18(b) refers to K_{II}. From Fig. 18, it can be seen that both K_I and K_{II} have similar changing tendencies at two crack tips. Also, K_I at the left tip is larger while K_{II} is smaller than those at the right tip. Since K_{II} is much smaller than K_I, the Mode I SIF at the left tip is more important for crack propagation. Our following discussions concentrate on the left crack tip. Fig. 19 shows the comparison of K_I and K_{II} at the left tip. It can be seen that the changing tendency of K_{II} with the external conditions is very similar to that of K_I. It also shows that K_{II} is much smaller than K_I. K_{II} tends to be zero with an increase in distance δ. This phenomenon is evident, as the applied loading is perpendicular to the crack face. So, the following analysis focuses on the Mode I stress intensity factor at the left crack tip.

Fig. 20 shows the variation of the normalized SIF K_I/K_I^0 with the normalized distance δ/a under the conditions $e_{13}E_3^0/\sigma_{22}^0 = -2.0$ and $e_{13}E_3^0/\sigma_{22}^0 = 2.0$, respectively. It can be seen that the variation of SIF with the external conditions is quite similar to that in the case shown in Fig. 8. However, Fig. 20 indicates that

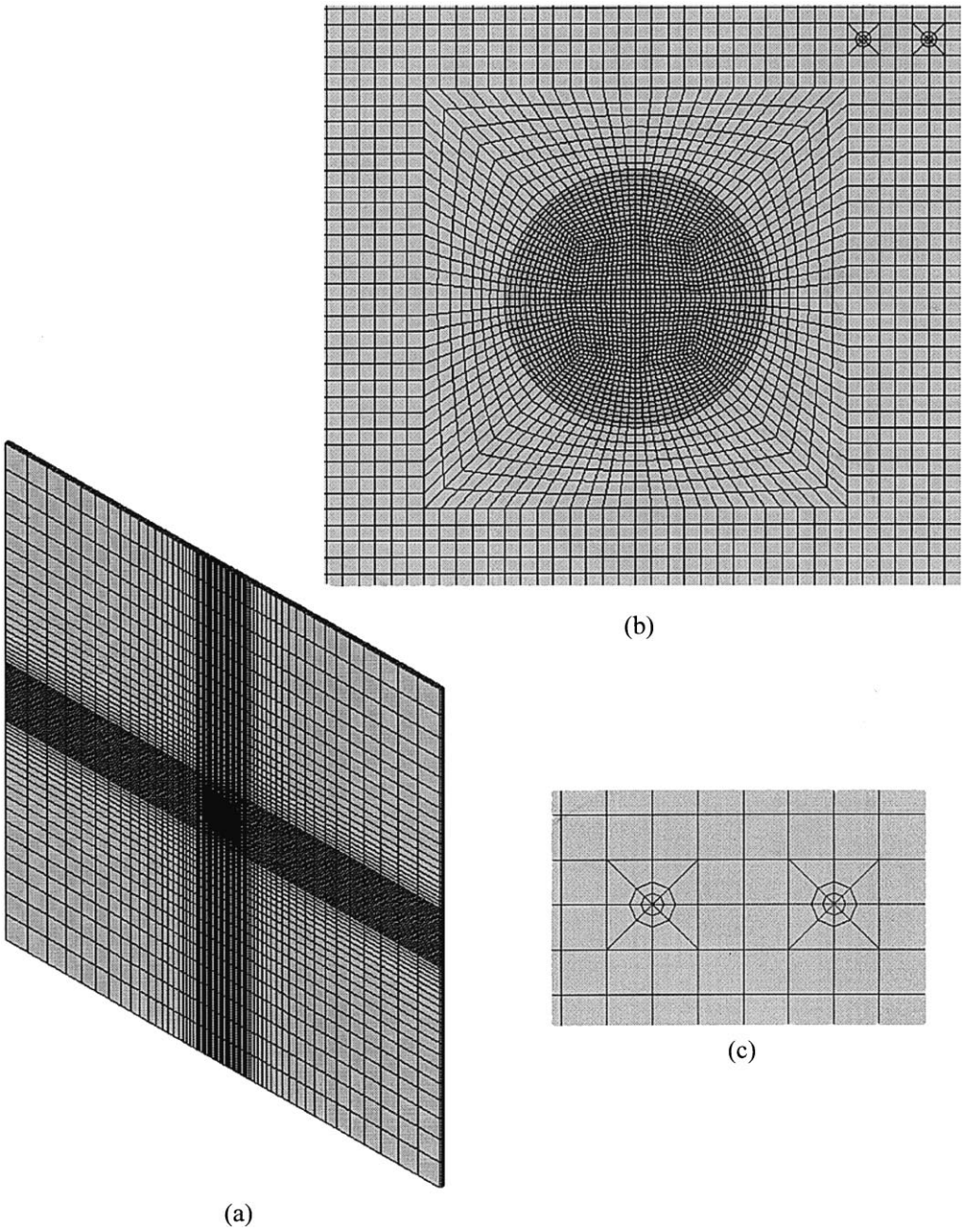

Fig. 15. The finite element model for the case of $\lambda = 45°$: (a) the overall 3-D mesh; (b) the plane view of mesh near the inhomogeneity–crack area; (c) the magnified mesh figure near crack tips.

for $m = 10.0$, the Mode I stress intensity factor K_I is always smaller than K_I^0, which means a "harder" inhomogeneity can shield the crack from propagating. However, when $m = 0.1$ and $\delta > 2a$, K_I is always greater than K_I^0, which means a "softer" inhomogeneity make the crack easier to propagate.

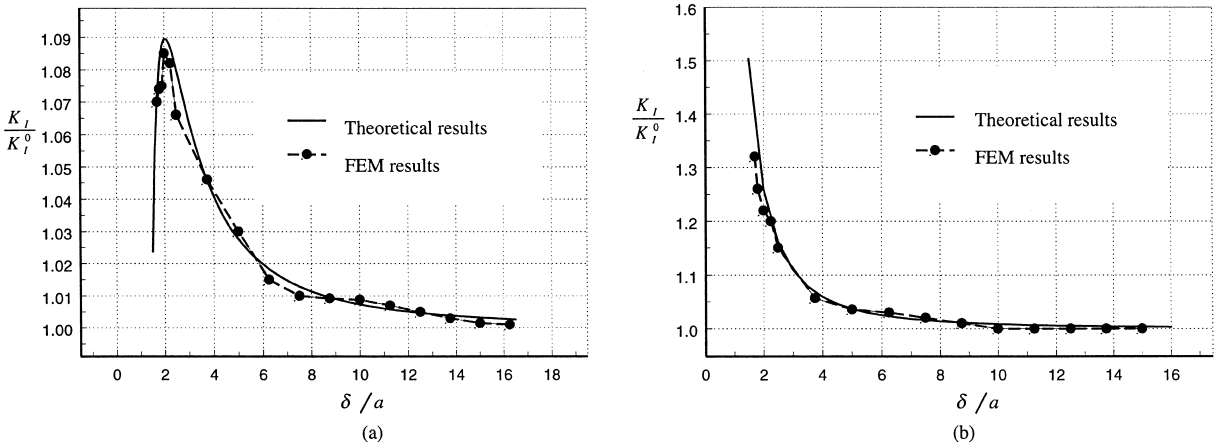

Fig. 16. Verification of K_{I} for $\lambda = 45°$: (a) $e_{13}E_3^0/\sigma_{22}^0 = 0.1, m = 0.1$ and (b) $e_{13}E_3^0/\sigma_{22}^0 = -5.0, m = 0.1$.

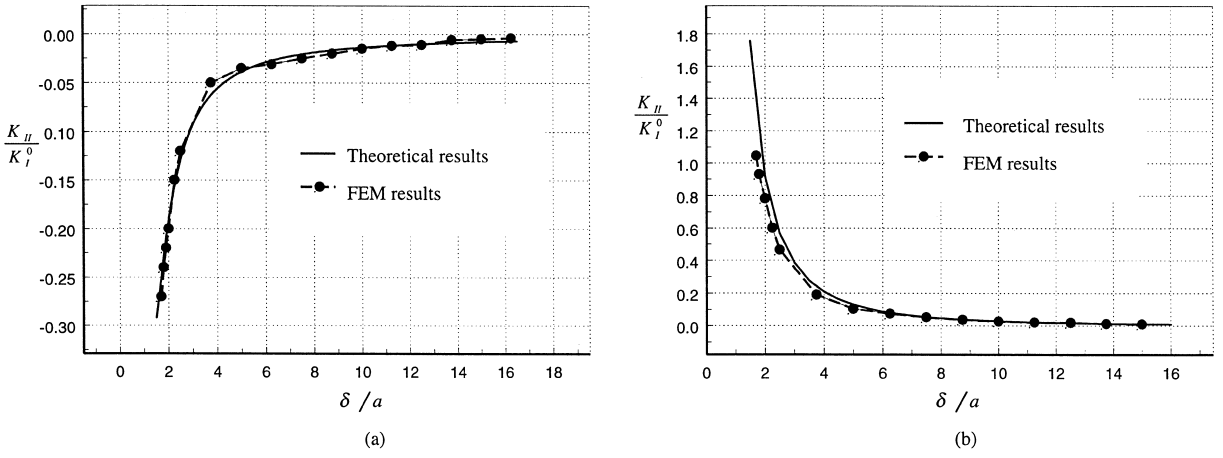

Fig. 17. Verification of K_{II} for $\lambda = 45°$: (a) $e_{13}E_3^0/\sigma_{22}^0 = 0.1,\ m = 0.1$ and (b) $e_{13}E_3^0/\sigma_{22}^0 = -5.0,\ m = 0.1$.

4.4. Comparison for the three configurations

To compare the inhomogeneity–crack interaction for the three configurations, Fig. 21 summarizes the variation of $K_{\mathrm{I}}/K_{\mathrm{I}}^0$ with normalized distance δ/a for the three cases. The following can be seen:

1. No matter where the position of the crack is, the influence of the inhomogeneity weakens with the increasing distance between them.
2. Under different normalized far-field electric loading $e_{13}E_3^0/\sigma_{22}^0$ and shear modulus ratio m, the variation of $K_{\mathrm{I}}/K_{\mathrm{I}}^0$ with δ/a at $\lambda = 45°$ is more stable than those at $\lambda = 0°$ and $\lambda = 90°$. The inhomogeneity has larger influence for $\lambda = 0°$ and $\lambda = 90°$ than that for $\lambda = 45°$.
3. When $\lambda = 0°$, the SIFs at crack tips increase as the far-field electric loading increases along the opposite x_3 direction, whereas the SIFs increase with the increasing electric loading along positive x_3 direction when $\lambda = 90°$.

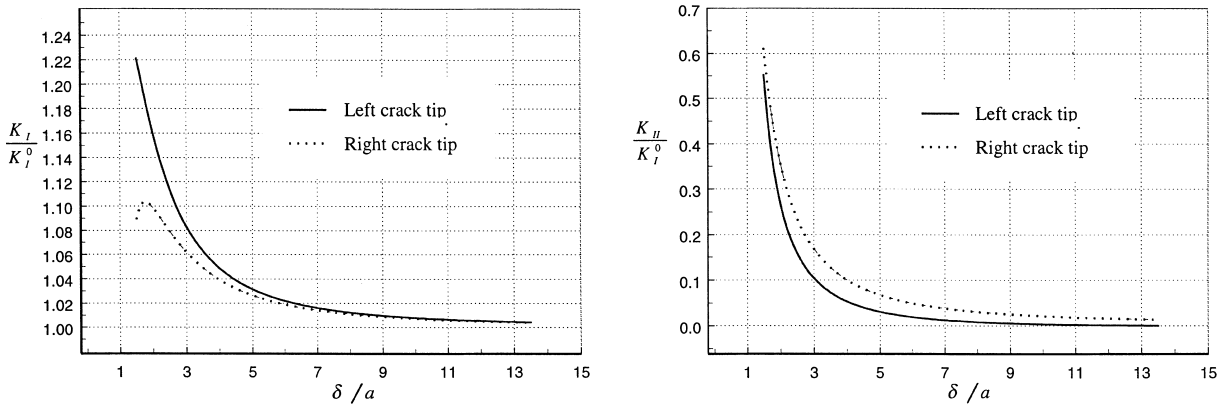

Fig. 18. Comparison of SIFs: (a) K_{I} and (b) K_{II} at the two crack tips under the condition: $e_{13}E_3^0/\sigma_{22}^0 = -2.0,\ m = 0.1$.

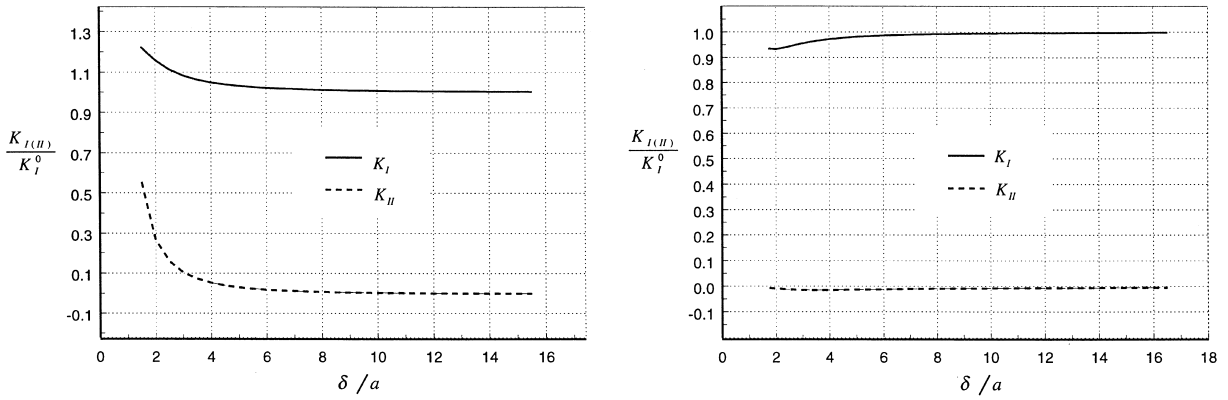

Fig. 19. Comparison of K_{I} andK_{II} at the left crack tip for $\lambda = 45°$: (a) $e_{13}E_3^0/\sigma_{22}^0 = -2.0,\ m = 0.1$ and (b) $e_{13}E_3^0/\sigma_{22}^0 = 2.0,\ m = 10.0$.

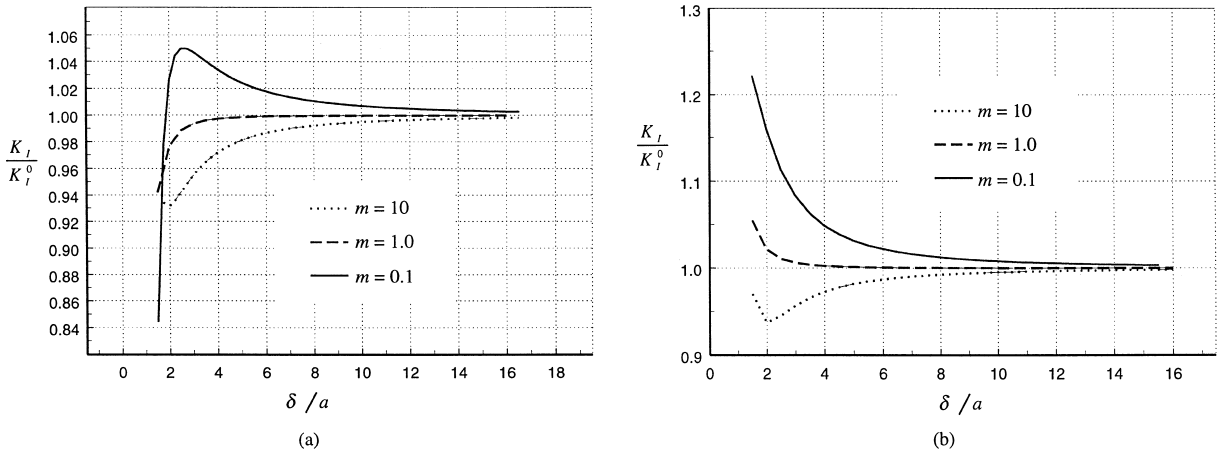

Fig. 20. Variation of K_{I} with δ at the left crack tip when $\lambda = 45°$: (a) $e_{13}E_3^0/\sigma_{22}^0 = 2.0$ and (b) $e_{13}E_3^0/\sigma_{22}^0 = -2.0$.

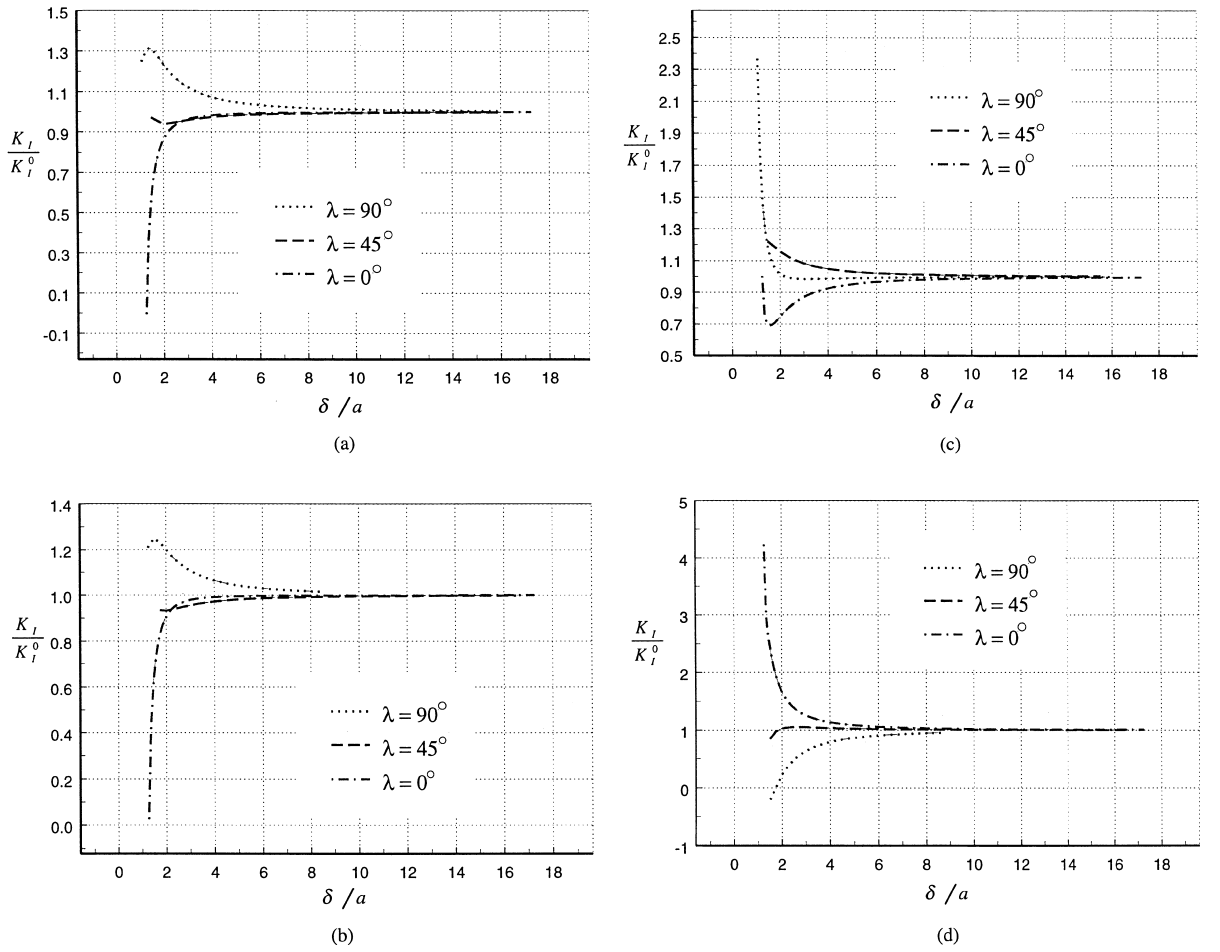

Fig. 21. Comparison of SIFs for the three geometrical configurations: (a) $e_{13}E_3^0/\sigma_{22}^0 = -2.0,\ m = 10.0$; (b) $e_{13}E_3^0/\sigma_{22}^0 = 2.0,\ m = 10.0$; (c) $e_{13}E_3^0/\sigma_{22}^0 = -2.0,\ m = 0.1$ and (d) $e_{13}E_3^0/\sigma_{22}^0 = 2.0,\ m = 0.1$.

4. When $\lambda = 90°$, the SIF increases with increasing material moduli of the inhomogeneity. In other words, the crack is easier to propagate with a "harder" inhomogeneity. When $\lambda = 0°$, a "softer" inhomogeneity can always make the crack easier to propagate.

5. Conclusion

The interaction problem of a cylindrical piezoelectric inhomogeneity embedded in an infinite non-piezoelectric matrix containing a crack is investigated. With the crack perpendicular to the far-field mechanical loading, three typical configurations are considered. The analytical solutions obtained have been verified through the finite element analysis. The investigations show that interaction between the crack and the piezoelectric inhomogeneity is influenced by the geometrical configuration, the far-field electric and mechanical loading, as well as the material properties of the inhomogeneity and the matrix. Numerical calculations on the interaction are carried out based on various influence parameters. Results obtained

might be applied on design of piezoelectric sensors to detect possible defects in solids or to use piezoelectric fiber to arrest crack propagation in composite materials.

Acknowledgements

The present work was supported by the National Science and Technology Board of Singapore.

References

ANSYS Analysis Guides. 000852, third ed., ANSYS Inc., 1995.

Dundurs, J., Mura, T., 1964. Interaction between an edge dislocation and a circular inclusion. Journal of Mechanics and Physics of Solids 12, 177–189.

Erdogan, F., Gupta, G.D., 1972. On the numerical solution of singular integral equations. Quarterly of Applied Mathematics 29, 525–534.

Erdogan, F., Gupta, G.D., Ratwani, M., 1974. Interaction between a circular inclusion and an arbitrarily oriented crack. ASME Journal of Applied Mechanics 41, 1007–1013.

Eshelby, J.D., 1957. The determination of the elastic field of an ellipsoidal inclusion and related problems. Proceeding of Royal Society A 241, 376–396.

Fan, H., 1995. A piezoelectric sensor embedded in a non-piezoelectric matrix. International Journal of Engineering Science 33 (3), 379–388.

Hills, D.A., Kelly, P.A., Dai, D.A., Korsuncky, A.M., 1996. Solution of Crack Problems, the Distributed Dislocation Technique. Kluwer Academic Publishers, Dordrecht.

Wang, B., 1992. Three-dimensional analysis of an ellipsoidal inclusion in a piezoelectric material. International Journal of Solids Structure 29 (3), 293–308.

Xiao, Z.M., Bai, J., 1999a. A close form solution for the stress field outside a circular piezoelectric inhomogeneity, Part I, On piezoelectric inhomogeneity related problem. International Journal of Engineering Science 37, 945–959.

Xiao, Z.M., Bai, J., 1999b. A circular piezoelectric inhomogeneity interacting with a nearby crack, Part II, On piezoelectric inhomogeneity related problem. International Journal of Engineering Science 37, 961–976.